# Virtual Endoscopy in Research and Clinical Practice

Dirk Bartz

Visual Computing for Medicine Group
University of Tübingen
Email: bartz@gris.uni-tuebingen.de

**Abstract**

*Virtual endoscopy is among the most active topics in virtual medicine and medical imaging. It focuses on the virtual representation of minimally invasive procedures for training, planning, and diagnosis without an actual invasive intervention. In the past few years, virtual endoscopy modes have been transferred from research systems in virtually every commercial medical imaging software, but with a varying quality and flexibility.*
*This report covers concepts used in current systems in research and products, and how they might be applied to daily practice in health-care. Specifically, I will start with an introduction into virtual endoscopy and the related medical field. This will also include typical scenarios of virtual endoscopy applications as they appear in clinical practice. This part will be followed by a discussion of the technical issues of virtual endoscopy and how are addressed in currently available systems. Among these issues are navigation through the respective body organ and the orientation aids for the users. Furthermore, I will highlight the different rendering techniques used and its impact on render speed and quality.*

Categories and Subject Descriptors (according to ACM CCS): I.3.7 [Computer Graphics]: Three-Dimensional Graphics and Realism J.3 [Computer Applications]: Life and Medical Sciences
***Keywords: Virtual medicine, virtual endoscopy, medical imaging***

## 1. Introduction

Minimally invasive procedures are of increasing importance in medicine because they have less deleterious effects on the patient. In particular, these procedures are used in gastroenterology, surgery, neurosurgery, (interventional) radiology, and many other fields. Usually, these procedures are performed using an endoscope, which is a fiber optic that is moved to the target area. The fiber optic itself can be flexible or stiff, depending on the size and other requirements of the endoscope. For instance, a typical endoscope for neurosurgery has a quite small diameter in order to minimize the impacted brain tissue. The small diameter reduces the possibilities to transport sufficient light through the fiber to the endoscope head. Building a stiff fiber to allow a maximum of light[29] compensates this effect. Beside the light source, an endoscope consists of the optic for a camera to transport the acquired image to a monitor, and has one or more "working tube" that are used to move tools such as pliers, to the target area. Cameras in the tip of the endoscopes have usually a large opening angle in order to provide a sufficient overview. Unfortunately, this also aggravates optical effects such as the fish eye vie[35].

Other tools for minimally invasive interventions include catheters, which are moved to the target area using a guidance wire - which gives the very flexible catheter stiffness - and fluroscopy/xray control that provides an overview of the current localization of it. A specific application area of catheter are (usually arterial) blood vessels. Note, that usual endoscopes cannot be used inside the examined blood vessels, since they are usually too large. Therefore, imaging is limited to the fluroscopy images, or provided by virtual endoscope, since a virtual camera cannot be too large.

Several drawbacks are associated with minimally invasive procedures. They are usually very unpleasant for patients, they are expensive (although they are still cheaper than "traditional" open surgery), and some areas of interest cannot be reached by the endoscope or catheter (due to folds and plaits). Especially in (neuro-) surgery, these procedures lack

the fast access for open surgery in case of serious complications, such as strong bleeding. Therefore, careful planning and realization of these procedures is essential, in order to avoid such complications. This problem aggravates, because handling and control of many of these endoscopes is very difficult, mainly due to limited flexibility of and limited field of view through the endoscope, a very limited depth perception, and the sensitive nature of the brain tissue.

In contrast, virtual endoscopy is a convenient alternative. It is based on a 3D scan of the respective body region. Examples for these scans are CT (Computed Tomography) scans, MRI (Magnet Resonance Imaging) scans of the abdominal area, the heart, the head, the lungs, or rotational angiography of blood vessels in various body parts. Based on the resulting volumetric data, the organs of interest are visualized and inspected from interior ("endo") viewpoints. Depending on the original endoscopic procedure, which is mimicked by virtual endoscopy, different goals can be achieved. These goals range from

- teaching: providing unusual insights into the anatomy of living patients,
- diagnosis: inspecting organs for (shape) defects, indicating unusual organ geometry,
- intervention planning: providing insight into the potentially complicated and non-standard anatomy of the patients and the individual organ location, and
- intra-operative navigation: currently, the position of a "real" endoscope is tracked by an infrared-based 3D navigation system and mapped into the image stack acquired previous to the operation. With virtual endoscopy, this position and orientation information can be exploited to provide a coupled visualization of optical and virtual endoscopy. In particular the virtual endoscopy can provide information which is not available to the optical endoscope, due to the limited flexibility and field of view.

In the next section, we propose a taxonomy of virtual endoscopy, based on its requirements and options for rendering and user-interaction. We will also classify the various approaches into that taxonomy. A more in depth discussion of these approaches will be presented in Section 4. We will also present a variety of applications, where virtual endoscopy systems – namely VIVENDI – have been successfully used (Section 5). Finally, we briefly discuss the advantages and shortcomings of virtual endoscopy in Section 6.

## 2. Requirements and Options for Virtual Endoscopy

### 2.1. Perspective Rendering

Mimicking endoscopy requires the rendering of the dataset with a strong perspective view inside of the dataset. Unfortunately, not all rendering algorithm – in particular the acceleration methods – can cope with these boundary conditions, and all algorithms suffer from the large magnification factors of perspective views inside of datasets and close to the rendered structures. Undersampling problems are almost always present and the limited resolution of the scanned datasets become often obvious. Some algorithms, however, are less prone to these problems. Isosurfaces reconstructed by the Marching Cubes algorithms [51] can be rendered with perspective views at no additional costs using graphics hardware. However, the large magnification factors and viewpoints close to these surfaces expose the typical diamond artifacts caused by the trilinear interpolation. Furthermore, the number of graphical primitives (triangles) generated by this approach is usually large. Several million triangles for large datasets are not uncommon. Therefore, the straightforward rendering of the triangles may be not possible at interactive framerates. Acceleration techniques like occlusion culling[45, 13] or surface simplification can ease that problem. Nevertheless, these techniques need to be applied with care, if image quality is traded off for the acquired additional speed.

Adaptive ray casting[61] can cope with the undersampling problem by adaptively oversampling the isosurface in these regions at the costs of lower framerates. Splatting[86, 59] enables filtered reconstruction of the voxels, but can also increase the blurriness of the representation[57]. The shear-warp algorithm [47] uses a base-plane approach that is generally not suited for large magnification factors encountered in virtual endoscopy, since the base-plane has the same resolution as the respective face of the volume dataset[57]. Even more recent improvements do not really allow these large factors[75].

#### Texture-mapping-based Volume Rendering

Texture-mapping-based volume rendering[25] suffers from various problems such as limited accuracy in the compositing pipeline – which might be overcome in announced graphics accelerators – limited texture/graphics memory that does not accommodate the whole dataset, and sampling problems[57] that are successively reduced.

To date, rich research has been investigated the use of texture mapping graphics hardware for volume rendering. In 1998, Westermann and Ertl presented 3D texture mapping-based volume rendering with isosurface shading [85]. Meißner et al. extended this approach with advanced clipping methods and shading of volumetric data[56]. In the past four years, many more researchers have improved the visual quality of texture mapping-based volume rendering. Engel et al. have coined pre-integrated volume rendering to address high reconstruction frequencies in transfer functions [31], which also enables to reduce the sampling rate to some extend. Other approaches use also the programmability of modern graphics hardware to improve the quality and the speed of this volume rendering approach [55, 64].

However, one of the major limits of texture-mapping-based volume rendering remains; since the full dataset rarely fits into the texture/graphics memory of the graphics accelerator, various swapping – ie., bricking – and compression

methods need to be applied. Overall, it does still not provide sufficient performance for interactive endoscopy applications. More details can be found in tutorials on texture-mapping based volume graphics[46, 30].

In summary, most virtual endoscopy systems use either an isosurface-based rendering using the graphics hardware, or an accelerated ray casting approach. In particular the latter one involves the exploitation of many auxiliary data-structures, like distance fields that need to be generated in a pre-process.

For a discussion of the cause and visual appearance of data and rendering artifacts[20], please refer to [10] (unfortunately only in German).

### 2.2. User-Interaction and Navigation Paradigms

Besides rendering, the used camera navigation paradigm determines the usability of a virtual endoscopy system. Controlling the camera in a virtual endoscopy application is not an easy task. The various approaches can be roughly classified into three classes[45]: automatic navigation, manual or free navigation, and guided navigation[36].

Many systems use a planned or automatic navigation, which generates an offline animation of a fly-through after specifying a camera path. This simple scheme reduces the interaction to a VCR-like functionality, requiring a costly refinement of the camera path (and of the animation), if the structure of interest is not well covered. In this context, Dachille et al. noted that only approximately 70% of the colon surface are covered by a single direction fly-through and up to 95% for a fly- through in both directions[26]. For the remaining parts, interactive camera control is required. A variation of the planned navigation is the "reliable navigation" [41], in which a complete "visit" of all structures of the organ is guaranteed. However, this also means that user interaction is limited and that irrelevant regions cannot be easily skipped. As an important cross-reference to the used rendering technique, automatic navigation does not require an interactive rendering technique, since the no user interaction lag is involved that could obstruct the navigation.

A manual or free navigation approach is another popular option. Unfortunately, the complexity of the anatomical structures commonly found in the datasets is very high. Even for a specifically trained physician, it can be difficult to navigate to the target. Furthermore, the unrestricted movement through the dataset imposes many view control limitations that render this approach as difficult to use[60]. For similar reasons, semi-automated fly-throughs[45] cannot be easily integrated into free navigation frameworks. Collision avoidance requires costly query operations and are therefore frequently not available in these systems. In contrast to automatic navigation, free navigation requires a highly interactive rendering technique, since a significant lag between interaction and rendering will severely disturb the user interaction.

Our final option is the guided navigation paradigm[36] that enables full navigation flexibility, combined with user guidance and an efficient collision avoidance scheme. Different techniques can be used to implement guided navigation. Galyean suggested a spring-based model to compute the respective constraints[36]. However, specific implementation details were omitted in this publication. In contrast, Hong et al.[45] used a several potential fields and a set of kinematic rules to implement their guided navigation system. While the original idea is to provide additional guidance the user, it can also be more constraint. Vilanova et al.[5] describe a guided navigation system where the location of the camera is fixed to a pre-computed path, while the camera orientation can be selected freely.

Guided navigation benefits from interaction rendering, since user interaction has an important role for the camera control. However, the guidance constraints are damping lags between user interaction and rendering. Therefore, a not very interactive rendering technique might be still usable. Nevertheless, a very slow rendering techniques that produces less than one or two frames per second is still not suited for guided navigation.

### 2.3. Taxonomy for Virtual Endoscopy Systems

In our taxonomy, we will focus mainly on the rendering techniques and camera navigation model used in the various systems. However, there are many more important features of the various systems, which we will not include in the taxonomy. Nevertheless, they can be very important too. Among these other features are: How well multiple materials/segmented objects are supported? How well the system is integrated in a PACS viewing system – a criterion that is very important for the daily clinical practice? How much pre-processing is required?

Table 1 gives an overview of the various systems classified by our taxonomy.

## 3. Related Work

Research on virtual endoscopy is one of the most active areas in virtual medicine. The various developed methods of virtual endoscopy have been applied to virtual colonoscopy[76, 45, 48, 5] (and other parts of the small and large intestines), bronchoscopy[77, 34, 63, 83, 54], ventriculoscopy[2, 15, 16], and angioscopy[27, 18, 38, 17, 11]. Other applications also include the ear/nose cavities[88, 66]. A more complete listing of applications of virtual endoscopy can is provided by Rogalla et al.[65, 67].

As mentioned before in Section 2.1, different rendering options can be used to trade off quality and rendering speed. Standard graphics hardware is used to render surface models[78, 52, 45, 13, 5, 60], extracted with the Marching Cubes algorithm[51]. However, the high geometric complexity of the extracted organ models frequently exceed

| Rendering Technique: Navigation Paradigm | Polygonal Surface Rendering With Accel. | Polygonal Surface Rendering No Accel. | Direct Volume Rendering High Quality | Direct Volume Rendering Reduced Quality |
|---|---|---|---|---|
| Automatic Navigation | | VESA[52],VirEn[5], 3D Slicer[37], FreeFlight[78] | VI VoxelView[69], PMS Endo3D, SMS Syngo | GE Navigator, SMS Virtuoso |
| Free Navigation | | FreeFlight[78], 3D Slicer[37] | PMS Endo3D, VI Vitrea2, SMS Syngo | GE Navigator, CRS4[38], SMS Virtuoso |
| Guided Navigation | VICON[45], VIVENDI[13] | VirEn[5] | Viatronix V3D Viewer | |

**Table 1:** *This table shows an overview of many of the available virtual endoscopy systems and their classification according to our taxonomy.*

the interactive rendering capabilities of most of the available state-of-the-art graphics accelerators, thus requiring either high-end systems[45, 78], algorithms to reduce the rendering complexity[45, 13, 42], or to relinquish interactive performance[18, 5].

Hong et al. [45] use a decomposition of the colon along its centerline. The resulting cell/portal structure is used together with a framebuffer-based visibility test to reduce the geometric complexity of the dataset to approximately 10%. To overcome the limitations to single-tube-like organ topologies, Bartz et al.[13] used an octree decomposition of the volume dataset and its isosurface in junks of roughly similar size. A hardware supported occlusion test is used to reduce the geometric complexity to 5-8% for a large variety of different organs. Hietala and Oikarinen[42] use a mixed technique, where a variation of template-based ray casting[87] provides visibility information later used for Marching Cubes-based polygonal rendering of tubular organ datasets (aorta and colon).

In contrast, volume-rendering techniques are used, partially for better visual quality, partially for interactive speed[73, 44, 27, 89, 38, 72]. Unfortunately, interactive speed has almost always compromised visual quality, general applicability, or flexibility. In [73, 69] and [44], key- framed animations are generated offline, which frequently leads to the time-intense refinement of the key-framed animation if the current camera path is not suitable. You et al. used a 16 processor SGI Challenge for parallel volume rendering of isosurfaces[89, 80]. However, image quality was still poor. In contrast, Gobbetti et al. used the 3D texture mapping hardware abilities of high-end graphics systems for volume rendering[38]. Here too, image quality was significantly reduced by the lack of shading.

The Navigator software of General Electric uses isosurface ray casting with roughly a few frame per second. Even if the performance of the 1996 results (one frame per second) has significantly improved, it hardly can be viewed as interactive[27, 34, 3, 2]. Similar solutions are provided by the Syngo platform of Siemens Medical Solutions (SMS) (Virtuoso was the previous 2D-texture-mapping based solution) and by the EasyVision Endo3D option of Philips Medical Systems[65, 20] (PMS) with similar performance of a few frames per second and varying image quality. Another variation was recently presented by Wegenkittl et al.[83], where six offline generated volume rendered movies were combined into a cube map to provide interactive rendering speed on low-end PCs similar to Chen's QuicktimeVR[22].

In terms of camera navigation paradigms, the various systems use all three options. Automatic navigation is used numerous systems[76, 44, 52, 69, 18, 41, 60] to generate an offline animation of a fly-through after specifying a camera path. Many systems with purely automatic navigation use direct volume rendering techniques, which provide high quality at quite low framerates[44, 69].

A free navigation approach is followed by Vining et al.[78, 76], Gobbetti et al.[38], and Nain et al.[60]. Typically, it is combined with the polygonal rendering of an extracted surface representation of the organs of interest[78, 60], since it requires interactive rendering performance. Most current commercial systems (GE Navigator, SMS Syngo, PMS EasyVision Endo3D) also provide a free as well as an automatic, path-based traversal of the structures of interest.

Finally, guided navigation[36] is used by Hong et al.[45] and Bartz et al.[13, 17] with full navigation flexibility. If no user-interaction is involved, the virtual camera moves along the pre-computed centerline to a specified target point. A more restricted fashion of guided navigation was introduced by Vilanova et al.[5]. Another variation of this more restricted guided navigation was presented by Wegenkittl et al.[83], where a cube mapped is used to generate an interpolated image from the pre-rendered six face of the cube, organized in six movies. Another image-based approach using a cube map was presented by Serlie et al.[72], which also combined a front and back view.

An interesting variation of virtual colonoscopy has been proposed in [40] and further developed in [8, 6]. Here, the colon is stretched and unfolded to provide an inspection mode sim-

ilar to pathology. This way, the whole colon can be examined without traversing it, therefore, no camera navigation model is required. Unfortunately, this technique is not easily adaptable to more complex organ systems with no simple tube-like structure like the colon. Even other tubular structures like blood vessel trees are not unfoldable by these techniques.

## 4. Detailed Look into Systems for Virtual Endoscopy

In this section, we will take a more detailed looked into a subset of available research systems for virtual endoscopy. In particular, we will examine the FreeFlight system of the University of Wake Forest[78], VESA of GE Corporate Research and Development, the VICON family of systems at the University of Stony Brook (SUNY Stony Brook)[45], the VIVENDI system of the University of Tübingen[13], and VirEn system of the Technical University of Vienna [5]. In addition, we will also briefly discuss a few other systems that have been developed.

Please note that detailed information of commercial products – as research spin-off or company developments – are usually not available. Therefore, some of the information provided in the next sections on these systems is by nature inaccurate and not necessarily describing the most recent state of these systems.

### 4.1. FreeFlight – University of Wake Forest

The FreeFlight system has been developed at the University of Wake Forest and is one of the oldest systems [78]. It is based on the OpenInventor API toolkit [74], which FreeFlight uses for interaction and rendering.

After the segmentation of the respective organ, a surface representation is generated using the Marching Cubes algorithm [51]. This surface representation is then used for the endoscopic examination where the user utilizes the interaction techniques of OpenInventor to explore the polygonal organ model. In addition to this free navigation mode, an automatic mode is also provided. It is based on a centerline algorithm that moves the camera through the organ cavity.

Next to the polygonal endoscopic view, FreeFlight is an early adopter of texture- mapping-based volume rendering [25]. However, its capabilities are limited by the size of the available texture memory and by the lack of shading. Finally, it provides the three orthogonal cross-sectional views of axial, sagittal, and coronal orientation. As approach to adapt to the actual rendering capabilities of the used graphics subsystem, FreeFlight offers the reduction of the volume dataset. However, the involved quality reduction can impact the proper representation of features such as polyps severely.

Overall, FreeFlight has the characteristics of a free navigation system with an isosurface-based rendering. The most severe drawback is surely the free navigation model that hardly provides sufficient functionality to provide an intuitive and easy to use interface for the potential users.

### 4.2. VESA – GE Corporate Research and Development

About the same time as FreeFlight has been developed, a similar system was developed at General Electric Corporate Research and Development. It was also based on the polygonal representation of surface of the segmentation of a selected organ. Algorithms from robot motion planning were used to generate a flight path through the organ, which then is used to move the camera through the organ model. Potential performance bottlenecks due to the large number of triangles in the surface representation could be overcome with polygonal simplification algorithms. However, this also involves the reduction of rendering quality and henceforth need to be used with great care.

By now, GE offers the Navigator module as the virtual endoscopy option for their Advantage Windows system. Based on the volume data of a patient, a ray casting approach is used to render the surface at a speed of a few frames per second[27, 3].

### 4.3. VoxelView/Vitrea2 – Vital Images (VI)

Also in the early years of virtual endoscopy (1994-1996), Vital Images developed the VoxelView system that was based on direct volume rendering (texture-mapped)[73, 69]. Pre-processing of the data volumes include the definition of the 8bit data window (from 12bit scanner data) and the resampling of the possible anisotropic volume into a isotropic grid. After the specification of the classifications through four transfer functions, a camera path is generated based on dedicated viewpoints, specified by the user, and a key-frame interpolation scheme. Afterwards, a video animation is generated in a time-intensive offline process. While the system provides a good image quality due to the used volume rendered method, it provides only a VCR like functionality of playing/replaying the video animation. If an important feature is not visible from the generated viewpoints of the camera path, it cannot be seen in the animation. Furthermore, a possibly need refinement of the camera path requires the regeneration of the animation, which took several hours at the time.

By now, Vital Images provides a different system in their Vitrea2 software. Here, they also provide a non-interactive manual navigation. This navigation mode is controlled by the cross-sectional viewer of Vitrea2 and steps slice by slice through the cavity. This conservative way of navigation is motivated by the traditional way radiologists examine data and is in contrast to most to other virtual endoscopy system which use either a world-frame control setting (ie., FreeFlight) or an endoscopic-frame setting. The rendering is based on a 2D/3D texture-mapping based volume rendering provided in Vitrea2.

As in most commercial systems, not only the software but the whole system at large is delivered in a completely configured computer system. Therefore, the rendering functionality is carefully tuned to the capabilities of the used graphics system. Currently, they are using a WildCat graphics accelerator.

### 4.4. VICON – SUNY Stony Brook

Early development in the VICON family of virtual endoscopy systems started in 1994 in the Vislab at the SUNY Stony Brook. It has its origin in an automatic navigation approach that generates an animation of a fly-through on a defined camera path[44]. In a pre-processing step, the start and end point of the camera path is specified by the user. After segmenting the respective colon region using a 3D region growing approach, the camera path is computed by calculating a centerline of that segmentation using "onion peeling", a thinning approach which successively removes outer voxels shells from the segmentation until only a one voxel wide connection remains. Thereafter, the direct volume rendering stage generates the respective animation.

Later, this approach was modified to adopt a guided-navigation paradigm[45, 36], in which the user can roam through the virtual colon as flexible as preferred. The used submarine model for intuitive guided navigation mimicked the submarine in the academy-awarded movie "Fantastic Voyage" where a miniaturized submarine traverses the blood vessel of a patient. Two (three) distance fields – interpreted as potential fields – are used for navigation purposes. The first one (two) implemented a forward (backward) stream from the start point to the end point, similar to the blood flow. The final distance field implements a collision avoidance system to prevent penetrations of the surface of the colon, based on the distance to the surface of the segmented voxels[70]. The distance field generation itself is interpreted as a single source graph problem where all voxels of the dataset represent the nodes of the graph and the voxel cell edges represent the graph edges. We used Dijkstra's minimum path algorithm [28] to calculate the forward (backward) distance field on the segmentation.

Together with a set of kinematic rules, which emulated the engine of the virtual camera/submarine, this model enabled an interactive and intuitive navigation through a colon. The distance fields are calculated on a 26-neighborhood of the segmentation of the colon. The default camera path – which the camera is following along the forward (backward) stream – is defined on a centerline calculated on the maxima and ridges of the collision avoidance (and forward) distance fields. This way, it enabled a smooth path in the center of the colon, if the influence of the two distance fields were parameterized accordingly[45, 9]. The very same approach was later re-discovered by the same group and described in [19] and yet again in [79]. After the segmentation and camera path have been calculated, the VICON system generated a subdivision of the segmented colon volume based on split planes of the three orthogonal orientations (axial, sagittal, coronal)[9, 45]. The isosurface was extracted using the Marching Cubes algorithm[51]. For the rendering of the isosurface during the interactive traversal of the colon, the split planes and remaining voxel segments were used as portals and cells for a potential-visible-set-based visibility algorithms[1]. Basically, this approach tests the intersection between the current and next portal from the current viewpoint for visibility. Here, contributions to the framebuffer are tested to establish if the geometry behind the next portal, represented by the respective cell, is visible and henceforth has to be rendered. Otherwise, it is skipped from rendering. Overall, this approach enabled a reduction of polygonal complexity of about 60% and enabled interactive rendering of more than 10fps on a SGI Challenge with an Infinite Reality graphics subsystem[45].

The VICON system has been constantly improved since the original, polygon-based approach. You et al. suggested to perform the direct volume rendering option – which uses ray casting – in parallel on a 16 CPU SGI Challenge[89]. Wan et al. [82] used the distance-to-surface distance field – used for the collision avoidance – to accelerate the empty space leaping using an approach similar to Zuiderveld's presented in [90]. Yet again, this approach was presented by Wan and Kaufman in [81]. In 2001, Li et al. also improved the rendering performance of the ray casting volume approach significantly. The original portal/cell approach is improved by employing cache coherence and the texture-mapping functionality of the graphics hardware[50] to limit the ray casting sampling to the visible surfaces. This way, he achieved a significant increase of rendering speed.

#### V3D Viewer – Viatronix

The technology of the previously described VICON system has been widely used in the V3D Viewer/Colon module of Viatronix. While the navigation module is still mostly based on the submarine guided-navigation system of VICON, its rendering technique has been improve quite a bit since the initial versions. Currently, V3D uses a variation of ray casting with a space leaping approach based on the distance field transform. Specific acceleration techniques exploit the close proximity of the inner organ wall, which saves empty samples of the rays casted from the viewpoint. Unfortunately, the high framerates break down, once the rendered surface becomes semi-transparent, requiring the sampling of the volume behind it.

Overall, V3D Viewer uses a highly optimized ray casting approach for rendering and – more or less – the previously known camera navigation paradigm of VICON.

### 4.5. Interactive Virtual Angioscopy – CRS4

An early texture-mapping-based approach[25] was presented by Gobbetti et al.[38]. Here, the volume data is rendered using

3D texture- mapping hardware, available on high-end graphics at the time. To adapt the distances between the slices to perspective projection, the slice space has been chosen inversely proportional to the actual distance. Furthermore, texture lookup tables are used to adapt the opacity of the samples accordingly[38]. The free navigation is accompanied with a force/friction model with is coupled with the opacity of the data samples. If the samples become opaque, this model detects collision and the respective collision reaction is calculated.

Overall, this system provided a few frames per second as rendering performance based on the texture-mapped volume dataset. If the volume dataset does not fit into the texture memory, a bricking technique is used to swap-in required parts of the dataset. In terms of quality, the system suffered from the typical poor rendering quality of the early texture-mapping-based volume rendering systems[25, 21] that lacked shading. Interaction follows to some extent the guided navigation paradigm, since collision avoidance is implemented based on the voxel opacities in the direction of the movement. Otherwise, it is a regular OpenInventor-type free navigation model.

### 4.6. VIVENDI – University of Tübingen

Similar to the V3D Viewer of Viatronix, the VIVENDI system developed at the University of Tübingen has its roots in the VICON system. It branched off after I left SUNY Stony Brook in late 1996 and has been modified and improved ever since. The major goal of the VIVENDI project was the reduction of the pre-processing times (which at the time required 10-16 hours) and to overcome the major limitation VICON was restricted to tube-like organs, due to its occlusion culling algorithm that is based on the segments of a colon. Furthermore, it integrated new functionality to navigate through complex multi-model scenes. Basically, the only similarity to the VICON systems is now the guided navigation systems, which is based on its submarine model[45].

The unsuited data structures are one of the major problems of the pre-processing stages of the VICON system. Consequently, we improved the heavily used priority queues by employing state-of-the-art structures of the LEDA library. Instead of the previously used FIFO queues, which are completely unsuited as implementation of priority queues with a large number of elements, we are now using Fibonacci heaps that reduced the computational complexity to $O(logN)$, in contrast to the $O(N^2)$ of the FIFO queue-based implemented[13]. Since the priority queues are used by Dijkstra's algorithm to compute the centerline and the forward (backward) distance fields, the respective run time could be reduced tremendously from many hours (almost one day) to a one digit number of minutes, even for large datasets. Similar results have been rediscovered by Wang[79].

To overcome the focus on tube-like organs, we replaced the centerline-based decomposition of the segmented volume by a spatial decomposition, based on an octree. Depending on the number of relevant voxels, voxels that contain the specified isosurface, the granularity of the leaf nodes of the octree is determined. This way, the decomposition is independent from the actual topology of the organ of interest and roughly balanced by the number of relevant cells that correlates roughly with the number of triangles. During run time, VIVENDI performs a hierarchical test on the tree nodes to establish if they are located within the view-frustum. This operation returns a front-to-back sorted list of the geometry organized in the leaf nodes of the octree, which is passed to the occlusion culling stage. Since the first 10% of nodes are rarely occluded, they are rendered without any occlusion test. All successive nodes are first tested for occlusion, based on their bounding volume, and depending on the result of that query rendered or skipped.

Currently, VIVENDI supports multi-object and multi-material interaction. Therefore, it can differentiate data from different segmentations with different connotations. In Section 5, we demonstrate the application in minimally invasive surgery planning in neurosurgery and a virtual bronchoscopy that exploit these features for the visualization of different structures.

VIVENDI has been successfully applied to a large number of different virtual endoscopy applications. See Section 5 for more details. For an in- depth discussion of the architecture of VIVENDI, please refer to [13].

### 4.7. VirEn – Technical University of Vienna

VirEn[5, 83, 4] has been developed over the past four years at the Technical University of Vienna in conjunction with Tiani MedGraph, a PACS system company. Similar to the previous two systems, it is based on a surface model of an organ, based on its segmentation in a volume dataset. It uses the Marching Cubes algorithm[51] to extract the surface model of the organ. In addition, it provides a ray-casted rendering of current viewpoints that provides better visual quality at significantly higher rendering costs. The rendering performance of the surface rendering depends on the selected graphics accelerator and might be not able to provide interactive framerates for large datasets.

The adopted navigation mode is a guided navigation, based on the centerline of the organ model. In contrast to VICON[45] and VIVENDI[13], the user navigation is limited. The virtual camera moves along the centerline of the organ. Only the view direction can rotate around the current camera position.

The centerline itself is generated by topological thinning, a process similar to the onion peeling[44], where voxel layers of a segmentation are successively removed as long as they preserve the topology of the voxels. This operation is computationally quite expensive and is done in a pre-process.

A variation of this rendering approach was presented by Wegenkittl et al.[83]. Here, the image generation is based on a cube-map of the volume rendered images of six viewing directions represented by the directions of the viewpoints along the camera path. Similar to Chen's QuicktimeVR[22], these six images are combined to generate the image of the current view direction. In Wegenkittl's approach, the views of the six view directions along the path a stored in six movies that are generated offline in a pre-process. At run time, they are interpreted as a cube-map to generate the display image. A similar approach has been proposed by Serlie[72], which in part is also integrated in the EasyVision system of Philips Medical Systems.

While VirEn uses a ray casting approach for direct volume rendering, the authors also suggested the use volume rendering hardware to accelerate the rendering. Since the used VolumePro system[62] does only provide parallel projection views, they decompose the volume in view direction in several slabs of several volume slices. These slabs are independently rendered by VolumePro and warped to simulate a perspective projection[7]. If the number of slabs is too low, the image quality suffers badly from the error introduced by the parallel projected slabs and their warping to fit the perspective projection[7]. To provide an acceptable quality, more than 130 slabs need to be used for a relatively small dataset of $256 \times 82 \times 105$ voxels. However, the multi-pass rendering of the different volume slabs reduces the performance of VolumePro significantly, since this is similar to the rendering of multiple volume datasets. For the mentioned number of required slabs (>130), the performance is less than 10 seconds per frame, a performance that is similar high-quality software volume rendering systems.

An interesting variation of virtual colonoscopy is unfolding the generated dataset into the plane. Vilanova et al. have proposed two different approaches how this unfolding can be achieved, while maintaining size ratios and overview in the generated images[8, 6]. Unfortunately, there are some situations where a colon fold can occluded a small polyp or other features. In these cases, the presented approaches will not represent that polyp in the unfolded colon properly. As noted before, this approach is not easily adapted to other organs with a less simple topology.

Overall, VirEn is a virtual endoscopy system that uses a surface-based representation of the organ structure. It uses a centerline-based approach to generate a camera path through the segmented organ. This camera path restricts the movement of the virtual camera and allows only the viewing direction to be selected freely. This can generate problems of inaccessible viewpoints, if the segmented structure has a complex shape. Furthermore, the rendering capabilities of the used graphics accelerator determine the rendering speed of the virtual endoscopy. If a large volume dataset is used and consequently a large polygonal organ model is generated, this can easily lead to non- interactive framerates of the virtual endoscopic inspection of the organ.

### 4.8. 3D Slicer – MIT and Brigham's and Women's Hospital

3D Slicer[37] is a joined effort of the AI Lab at MIT and the Surgical Planning Lab at Brigham's and Women's Hospital in Boston. It is software for medical imaging, which performs segmentation of organ structures from volume data, and the respective 3D rendering of these structures. In addition, it provides the traditional 2D orthogonal cross-sections of the volume dataset. 3D Slicer itself is based largely on VTK[71] and offers no additional acceleration techniques to improve the rendering performance beyond the offerings of the used graphics hardware. However, VTK also provides surface simplification mechanisms that can be used to generated a less complex model of the organ. In turn, that also reduces the fidelity and accuracy of the generated surface model.

Nain et al.[60] recently added a virtual endoscopy viewing mode to 3D Slicer, which uses a surface model of the segmented organ to render the endoscopic view. In addition, it provides the three orthogonal cross-sections of the current viewing position. As a special feature, these cross-sections are not necessarily aligned with the volume dataset, but can be multi-planar reformatted representations (MPR), aligned with the current viewing orientation.

Three different modes of navigation are provided; two automatic navigation modes, and one free navigation mode. The first automatic mode is based on a key-frame interpolated path of viewpoints – called landmark by Nain et al.[60] – specified by the use. The derived viewing direction depends on the travel direction. Unfortunately, this way automatic navigation usually suffers from the gimbal lock, since the roll of the virtual camera is not really specified[45]. The second automatic navigation mode is based on a centerline generation, using temperature distribution functions and their finite- element-based numerical solution[60]. While the authors claim that this centerline can be generated with minutes on a Sun Ultra 10 workstation for a dataset of approximately 100K triangles, the performance on to date datasets of more than a million triangles per dataset is unclear.

Finally, 3D Slicer provides a free navigation mode. While the authors describe the difficulties of freely navigating through a model similar to the FreeFlight system, they propose to use a 3D gyro structure to aid the user for accurate navigation[60]. Furthermore, they provide an endoscope local reference frame that also improves the handling of the virtual camera. Collision avoidance is implemented by measuring the distance from the current viewpoint in view direction to the surface. If the user-specified threshold is reached, the appropriate reaction is calculated.

Overall, 3D Slicer provides a surface-based rendering

model with a performance that completely depends on the polygonal complexity of the model and on the rendering capabilities of the used graphics hardware. The adopted free navigation approach only ease the problems of free navigation. The used o 3D gyro or the local reference frame still appear to be more cumbersome than the submarine model used in VICON[45] or VIVENDI[13].

## 5. Applications of Virtual Endoscopy

In this section, we present various virtual endoscopy applications of VIVENDI[13]. Specifically, we will look into virtual colonoscopy (next Section), virtual ventriculoscopy (Section 5.2), virtual angioscopy (Section 5.4), and virtual bronchoscopy (Section 5.5).

### 5.1. Virtual Colonoscopy

Originally, virtual colonoscopy used the VICON system [9, 45] with application specific algorithms for occlusion culling and volume rendering. Unfortunately, these algorithms depended on the tube-like topology of the colon which circumvented the utilization of VICON for other application areas. However, the VIVENDI system[13] does not have these limitations. As described earlier, it uses an octree-based decomposition of the isosurface extracted from the volume dataset. The octree structure can be seen in Figure 1. The individual blocks of the colon of the patient dataset are rendered in different colors. In the remainder of this section, we repeat the results already reported in[45] for the sake of completeness. This time, however, we use the VIVENDI system which has a more flexible lighting model, which enables a spotlight at the camera position pointing in the view direction.

#### 5.1.1. Motivation

Cancer of the colon and rectum is the second leading cause of cancer deaths in the USA. Approximately 150,000 new cases of colorectal cancer are diagnosed every year[24]. Consequently, it is imperative that an effective diagnostic procedure is found to detect colonic polyps or tumors at an early stage. Currently, optical colonoscopy and barium enema are the major procedures available for examining the entire colon to detect polyps larger than *5mm* in diameter, which are clinically considered to have a high probability of being malignant. In optical colonoscopy, a fiber optical probe is introduced into the colon through the rectum. By manipulating the tiny camera attached to the tip of the probe, the physician examines the inner surface of the colon to identify abnormalities. This invasive procedure takes about one hour and requires intravenous sedation, resulting in high costs. Barium enema in contrast requires a great deal of physical cooperation from the patient when the X-ray radiographs of the colon are taken at different views. Additionally, its sensitivity can be as low as 78% in detecting polyps in the range of *5mm* to *20mm* [58].

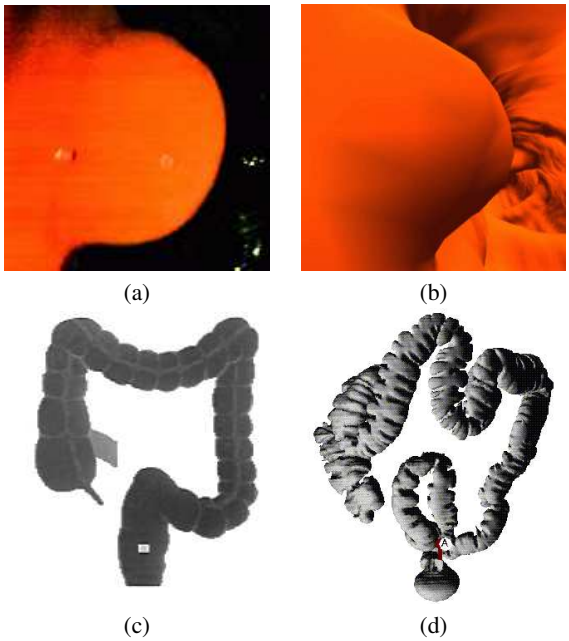


**Figure 2:** *An 8mm polyp in the descending colon, close to the Sigmoid colon; left (a,c): optical colonoscopy, right (b,d): virtual colonoscopy* [45].

Both methods are either too expensive or to circumstantial for prophylactic screening examinations – resulting in a low patient acceptance –, hence virtual colonoscopy was proposed to limit optical colonoscopy to cases in which either a suspicious polyp was found – which induced a biopsy or removal of the polyp – or which were inconclusive in virtual colonoscopy [76]. The latter happens if (shape) defects of the graphical representation of the inner colon surface cannot be identified as polyps or residual stool. A study on the advantages of virtual colonoscopy compared to optical or conventional colonoscopy has been presented by Fenlon et al.[33]. The authors found that the performance of virtual colonoscopy is comparable to optical, as long as the data resolution is sufficient to detect polyps of the respective size. Problems arose from residual stool, which often was the cause of a false positive finding.

After cleansing and inflating of the colon (both actions are also required for optical colonoscopy), a CT scan (or alternatively an MRI scan) is performed. The resulting image stack is pre-processed and examined using the VIVENDI system.

#### 5.1.2. Optical and Virtual Endoscopy

We compare the results of optical and virtual endoscopy based on polyps found in both procedures. In particular we compare snapshots of two polyps (see Fig. 2 and 3). The first polyp (Fig. 2) is located in the descending colon, close to

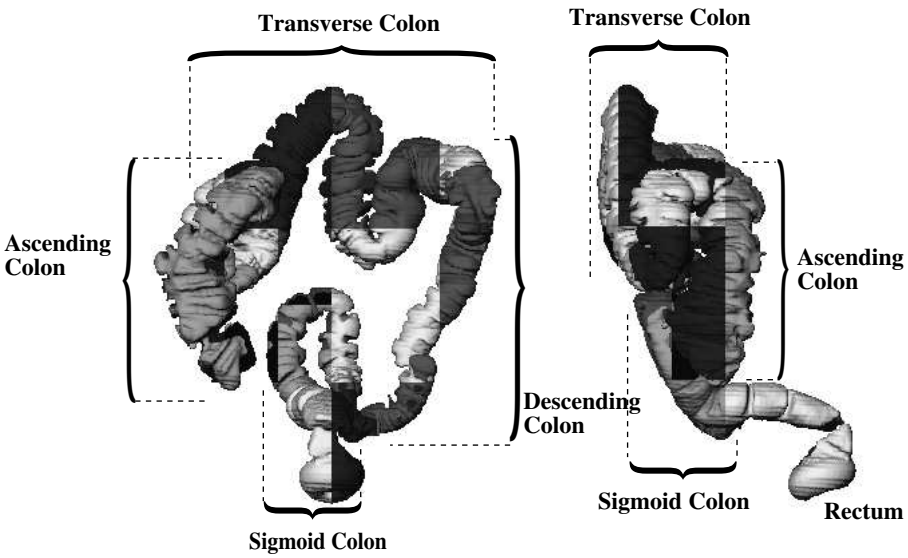


**Figure 1:** *Octree-based decomposition of colon dataset; the octree leaf blocks of the isosurface are represented with different colors. The left image shows a coronal view, the right image shows a sagittal view.*

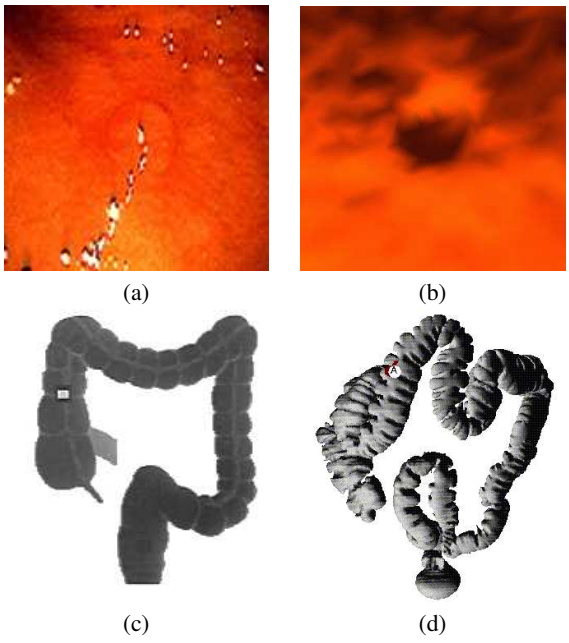


**Figure 3:** *An 4mm polyp in the transverse colon.; left (a,c): Optical colonoscopy, right (b,d): virtual colonoscopy* [45].

the sigmoid colon. It is of a size of 8mm and hence of high clinically relevance. Figure 2a and c show the information provided by optical colonoscopy, while b and d show the information provided by virtual colonoscopy. The shape information of the polyp is well represented by the virtual technique. However, textual information is not available, while it is very helpful in optical colonoscopy (although not obvious in Fig. 2a or 3a).

The overview image of virtual colonoscopy (Fig. 2d) provides much better information than for optical colonoscopy, which is just a rough sketch of the general shape of a colon (Fig. 2c). In particular the position information of the polyps can be misleading – optical colonoscopy estimates the position of the polyp in the sigmoid colon (see Fig. 2c), while it is accurately reconstructed in virtual colonoscopy – locating the polyp in the descending colon.

The second polyp is of a size of 4mm and it is located in the transverse colon, not too far away from the hepatic (right) flexure. Similar to the previous polyp, the actual location is quite different from the rough estimation in the overview image of optical colonoscopy, which locates the polyp in the ascending colon.

To summarize, virtual colonoscopy is an alternative procedure for the diagnosis of polyps in the human colon. However, it does not replace optical colonoscopy, which is still required once a found polyp has to be removed or a suspicious structure needs to be identified with additional information, such as texture, color, and histological information through a biopsy, which is generally not available by means of volume scanning methods,

Other applications of virtual colonoscopy include teaching, planning of optical colonoscopy procedure, and of intraoperative navigation.

### 5.2. Virtual Ventriculoscopy

The focus of (optical and virtual) ventriculoscopy is the ventricular system of the human brain, where the CSF (cerebrospinal fluid) is produced and resorbed (Figure 4a). Specifically, the CSF is produced in the lateral (upper two) ventricles. Due to respiration and other metabolistic activity, the CSF flows through the *foramen of Monro* into the third ventricle (which is also producing CSF), and via the narrow connection of the ventricular (cerebral) aqueduct to the lower fourth ventricle. From this ventricle, the CSF is distributed to other cavities inside of the skull.

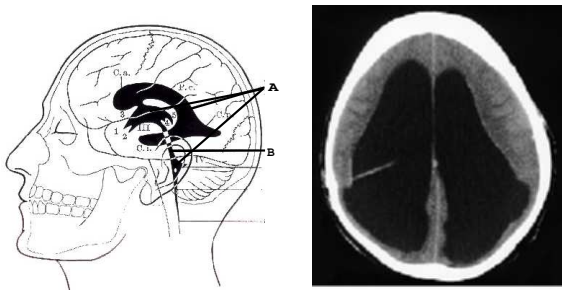


(a) (b)

**Figure 4:** *Ventricular system of the human head*[68]*: (a) A ventricles, B ventricular (cerebral) aqueduct, (b) Hydrocephalus in an image from a CT scan*

#### 5.2.1. Motivation

The drain of the third ventricles into the fourth ventricles is often blocked, due to occlusion or a stenosis of the aqueduct. This can be caused by a tumor, an accident, meningitis, or a congenitally defect. The result of such a blockage is a serious disturbance of the natural flow of the CSF, which frequently leads to a dangerous increase of pressure inside the skull and can damage the brain severely (Fig. 4b).

The standard procedure for this hydrocephalus is the external drainage of the ventricular system into the abdominal cavity using a shunt. Unfortunately, this external drainage system is frequently the cause of complications – such as obstructions and degenerative processes – which result in the needed neurosurgical replacement of the shunt. Furthermore, the missing natural flow of CSF leads to degenerative processes of CSF producing structures and the resolving of the septum between the lateral ventricles. The treatment of the basic cause of the occlusion is usually not possible, because of the inaccessibility of the aqueduct for neurosurgical instruments. Recently, a new endoscope – small enough to pass through the foramen of Monro and with enough luminous intensity – was developed which allows interventions inside of the ventricular system [29]. In consideration of the inaccessibility of the aqueduct – even with the new endoscope – the department of neurosurgery of the University Hospital at Tübingen is performing a *ventriculostomy*, where the natural drain via the aqueduct and the fourth ventricle is bypassed by a new drain in the floor of the third ventricle. To access the ventricles, a hole is drilled through the skull and a tube is placed through this hole, through the brain, into the posterior horn of the left or right lateral ventricle. Thereafter, the endoscope is introduced through the tube, which is used as a stable guide for the endoscope. It proceeds forward through the foramen of Monro to the floor of the third ventricle.

Because of the water-like optical property of the CSF - which fills the ventricular system, viewing of the surrounding tissue is possible. Movement of the endoscope – guided by video-control via the small field of view of the endoscope – is limited by the tube and the surrounding tissue. Micro-instruments, introduced through an additional canal inside the endoscope, can then be used to perform the actual minimally-invasive procedure, ie., removing accessible mass lesions. In the case of a ventriculostomy, the thin membrane of the *lamina terminalis* is perforated, thus realizing a new CSF perfusion balance.

Other indications for minimally-invasive procedures include the formation of a CSF-filled cyst which also introduces pressure on blood vessels, nerves, or the ventricular aqueduct. To avoid these dangerous increases of pressure inside of the skull, the cyst is drained using the endoscope.

#### 5.2.2. Virtual Endoscopy of the Ventricular System

The major problem of procedures as described above is the limited view and orientation through-out the intervention which increases the necessary time of the intervention and consequently, the inherent risks of serious complications. To overcome these drawbacks, we propose the use of a virtual endoscopy system to improve the planning of and orientation during this procedure [13, 15].

Based on pre-operative acquired MRI/3D CISS (Constructive Interference in Steady States) scans of the patient's head, the respective ventricular system is reconstructed and examined by the VIVENDI system. In particular the access ways to the target areas – ie., the floor of the third ventricle – are explored to optimize the optical neuroendoscopic procedure. Besides the planning of neuroendoscopic interventions, virtual neuroendoscopy can also be applied to explore the stenosis of the ventricular aqueduct, an area which is not accessible with the endoscope. Figure 5 shows various snapshots from virtual ventriculoscopy; the position and orientation of the virtual camera is represented in the lower row of Figure 5. Each snapshot visualizes important anatomical structures, such as the *choroid plexus*, which is responsible for the production of CSF, and the *choroid plexus vein*, which is supplying the choroid plexus in Figure 5a. The entry point for the endoscope into the third ventricle is shown in Figure 5b. The pipe-like structure of the *adhesio intertha-*

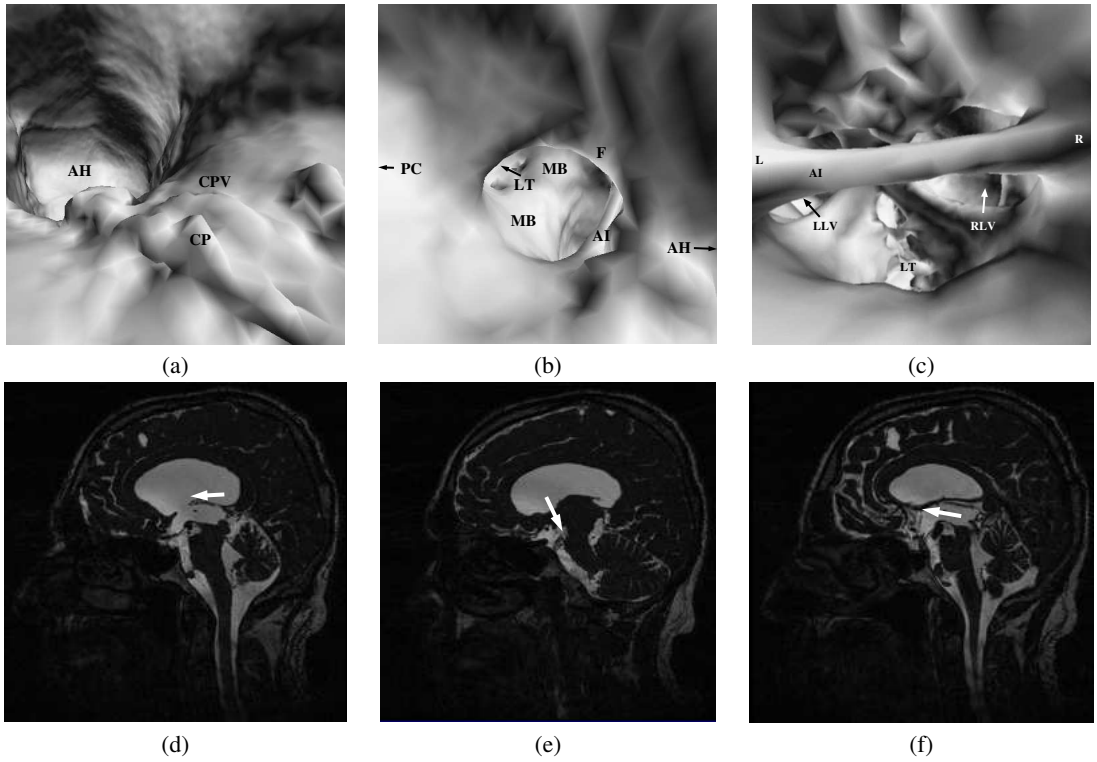


**Figure 5:** *Virtual Ventriculoscopy; upper row – endoscopic view, lower row – MRI/3D CISS orientation slice. (a/d) Left lateral ventricle, approach from posterior horn via pars centralis (PC) to anterior horn (AH); (b/e) foramen of Monro, approach via right lateral ventricle; (c/f) foramen of Monro, approach from third ventricle; CP = choroid plexus, CPV = choroid plexus vein, F = fornix, AI = adhesio interthalamica, MB = mamillary bodies, LT = lamina terminalis, LLV = entrance to left lateral ventricle, RLV = entrance to right lateral ventricle*[15].

*lamica* connects the *thalamus* through the third ventricle. The upper bending of the foramen of Monro contains the *fornix*, which belongs to the *limbic system*. The limbic system is involved in the learning process which renders the fornix as a very sensitive part of the body. If it is injured by the endoscope while it enters the third ventricle, a severe learning disability can be the result. The *mamillary bodies* in the floor of the third ventricle, also belong to the limbic system. Figure 5c shows a view from a view-point which is already not accessible for an optical endoscope. It visualizes another important structure in the floor of the third ventricle, the *lamina terminalis*, which is a thin membrane between the third ventricle and the basilar cistern (or sometimes also referred to as cistern of the lamina terminalis). This membrane is the target area for the new CSF drain of the ventricular system.

Another application for virtual endoscopy is as a 3D navigation aid to complement the current slice based navigation which tracks the tip of the endoscopic instruments and maps their registered position into the MRI dataset. The position and orientation derived from this navigation system can be loaded into VIVENDI to synchronize optical and virtual endoscopy. If a complicated anatomical situation is experienced, the area can be virtually explored using VIVENDI to determine the appropriate action. Figure 6 shows the (manually) matched display of optical (a, c) and virtual (b, d) endoscopy of two different datasets. Only the geometric shape information is captured by the MRI scan; all texture information, such as blood vessel color, surface color, is not available to virtual endoscopy.

### 5.3. Multi-modal Visualization for Neuroendoscopic Interventions

One of the most dreaded complications of minimally-invasive neurosurgery are lesion of blood vessels. Even if only a small blood vessel is injured, the resulting bleeding ("red-out") causes a sudden loss of optical visibility through the endoscope which introduces severe difficulties for obtaining the desired results of the interventions. A more dangerous situation arises if a major blood vessel is injured. A lesion of an artery results in a fatal mass bleeding, an usually lethal outcome of an intervention.

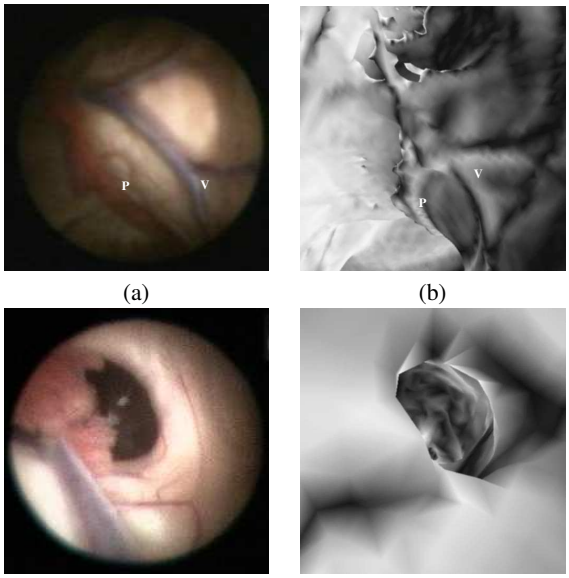


**Figure 6:** *Manually matched views from optical and virtual ventriculoscopy. (a, b) show the thalamostriate vein (V) and choroid plexus (P) from the right lateral ventricle. (c, d) show the right foramen of Monro, including the choroid plexus vein (Fig. 5a) and the choroid plexus structure.*

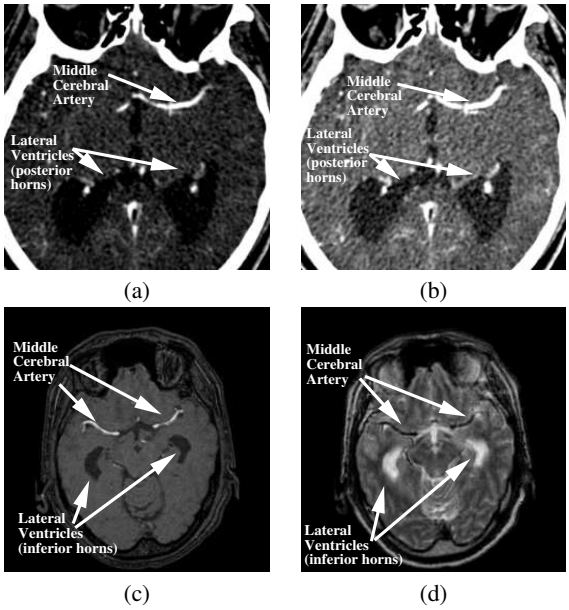


**Figure 7:** *Upper row: CT axial slice with the posterior horns of the lateral ventricles and middle cerebral artery with two contrast windows (a, b). Lower row: MRI axial slice with the inferior horns of the lateral ventricles and middle cerebral artery (left and right). (c) MRI angiography sequence, (d) MRI TSE sequence* [16].

Unfortunately, the major basilar artery is located directly below the floor of the third ventricle without an optical visibility from the third ventricle. To avoid traumas of such blood vessels, we modified the VIVENDI-framework[13, 17] to represent multiple anatomical information of the patient data using several 3D scanning techniques[16]. For the rendering of this multiple anatomical patient data, VIVENDI provides frame-rates of more than 25 fps on an HP J7000/VISUALIZE fx6 workstation, and about 20 fps on an HP P-class/VISUALIZE fx6 PC running LINUX.

### 5.3.1. Matching Different Data Modalities

To visualize different anatomical structures, different scanning modalities and protocols are required. The associated volume datasets vary in terms of orientation, resolution, voxel dimensions, translations, and rotations. For a combined visualization of these datasets matching parameters need to be found, which is a very difficult procedure. To minimize the necessary matching expenditure, we conducted several experiments to determine an appropriate scanning protocol, based on CT and MRI scans. For the targeted application, two anatomical structures need to be identified; the CSF-filled ventricular system and cysts, and the blood filled major arterial blood vessels in proximity to the CSF-filled target areas.

The (contrast agent-enhanced) CT scan provided a good contrast and a high resolution for the vascular system within the region of interest. However, this CT scan did not produce a sufficient contrast between the brain tissue and the CSF-filled cavities, while still preserving the complete inner surface of the cavities (Fig. 7a and b). Furthermore, CT inherently introduces radiation, an additional drawback compared to MRI. Blood-flow induced MRI angiography (Time

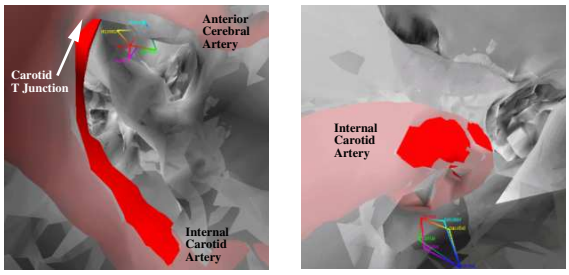


**Figure 8:** *(a) Close-up to internal carotid artery. (b) View downwards on the "carotid siphon", below the carotid T junction*[16].

of Flight/TOF, Fig. 7c) also reconstructs the vascular system with good quality, although the resolution is slightly lower

than with a CT scan. However, it is not usable for the segmentation of CSF-filled cavities, since the ventricular system cannot be separated from the space surrounding the skull. Therefore, we perform a second MRI scan that focuses on these cavities right after the MRI angiography. We previously (see Section 5.2) used an MRI 3D CISS sequence to reconstruct the ventricular system in patient datasets. Unfortunately, the different scanning orientation (sagittal/3D CISS and axial/TOF) introduced a surprisingly difficult match procedure, which qualified this sequence as impractical. Similar problems prevent a combination of MRI volumes with CT volumes, since different patient positioning and field of views pose almost insuperable matching problems. Consequently, we modified the 3D CISS sequence to an MRI TSE sequence (Turbo Spin Echo, Fig. 7d) to reconstruct the cerebral ventricles, which provides the same orientation as the angiography sequence and unfortunately, also a smaller slice range than the 3D CISS. However, it turned out that the resolution is sufficient for our purposes. Finally, the combination of MRI angiography and MRI TSE data delivered a satisfying matching and image quality and was henceforth used in all later experiments. Furthermore, MRI does not expose radiation, in contrast to a CT scan.

Both sequences were performed subsequently, without changing the position and orientation of the patient. It later turned out in our experiments that patient movement during both scans is negligible. Although the resolution within the axial slices is twice as large in the MRI angiography as in the MRI TSE sequence, the scans generate two well-aligned data volumes. However, the number of axial slices in the MRI data is different, and hence so is the covered scanning area. This difference requires a manual slice matching step that is performed by a neuroradiologist or neurosurgeon. The calculated axial translation generates an error which is at most the distance between two slices in the data volumes. A manifestation of this error can be found in Figures 8 and 9, where the red/dark, as opaque rendered artery geometry reconstructed from the MRI angiography sequence penetrates the geometry of the as transparent rendered CSF-filled cavity geometry[†]. Especially in Figure 9a, the "original" position of the blood vessel is also visible in the geometry extracted from the MRI TSE sequence. Fortunately, the maximum error (if the matching step is correct) is always sufficiently below a critical threshold, where the "clearance area" would also cover the proposed target area of the endoscope. Figures 10 and 11 show a different dataset of a patient who was subject of a ventriculostomy.

Currently, the VIVENDI system is now providing the vascular topography combined with the information of the anatomical structure of the CSF-filled ventricular cavities. This information is successfully used to represent the location of the blood vessels to carefully plan the neuroendoscopic intervention. Lesions of the respective arteries can be avoided, resulting in a substantial reduction of the risk of serious complications.

[†] The depth sorting of the geometry for correct transparent rendering is obtained by the view-frustum culling; all subdivision entities are sorted according to their closest depth values.

### 5.4. Virtual Angioscopy

The blood circulation system is of special interest for physicians, since many injuries and diseases of this organ system can result in serious, potentially life-threatening conditions. Many of the diseases cause stenosis or aneurysms of the blood vessels. Both developments can be assessed using virtual endoscopy methods. These methods can be particularly useful in diagnostic applications where interior explorations using "real" endoscopic tools are not possible.

#### 5.4.1. Data Acquisition

Currently, the major method for the visual representation of the angio-architecture is by 2D angiography, where a contrast agent is injected via an endovascular catheter. A subsequently taken X-ray radiograph (DSA or fluoroscopy) acquires a 2D projection of the vessels, which are of high resolution but lack spatial information.

Alternatively, other non-invasive techniques are available to visualize vessel trees in 3D. CT angiography techniques also require the injection of a contrast agent. The major drawbacks of this method are the limited resolution in Z (slice distance) and motion artifacts due to patient movements. These problems are reduced or even eliminated with the new CT multi-slice technology (ie., Siemens SOMATOM Volume Zoom) which enable isotropic data volumes and less motion artifacts due to faster scanning, possibly triggered by a heart monitor for cardio-vascular imaging.

MRI angiography is based on the flow-induced data and hence, it does not require the injection of a contrast agent. Furthermore, it does not introduce radiation in contrast to CT-based angiography. However, the lower resolution and the relatively long scanning time of 20 minutes make MRI-based angiography sensitive to patient movement and virtually impossible to use for fast moving organs, ie., the heart. Additionally, some MRI angiography sequences might introduce fake stenosis, due to measuring artifacts[23].

Another advanced technique is *rotational angiography* [32, 39], where up to 140 X-ray-based projections are taken from a rotation range of 200 degrees around the patients. Based on these individual projections, a 3D volume is reconstructed which represents the respective blood vessels (if a contrast agent is injected) and other anatomical structures in very high resolution. However, the relatively short scanning times of up to 13 seconds make rotational angiography still too slow for fast movements (ie., heart beat).

Currently in clinical practice, the examinations of the

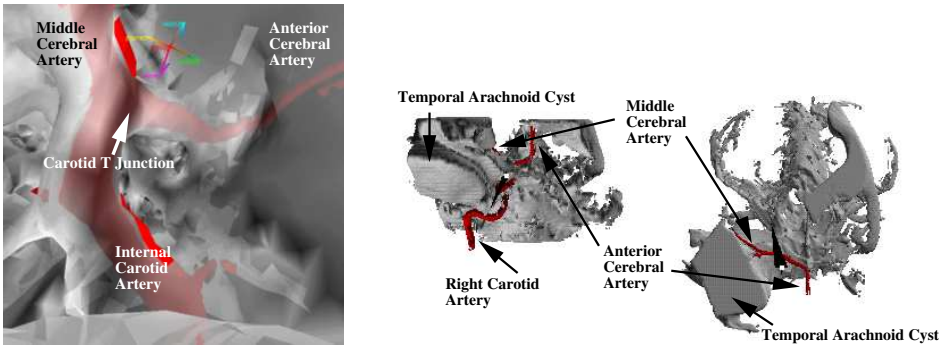


(a) (b)

**Figure 9:** *Temporal arachnoid cyst dataset: (a) View on to carotid T junction, where the internal carotid artery branches into the lateral middle cerebral artery and the frontal anterior cerebral artery. The red vascular geometry – extracted from MRI angiography – penetrates through the visible vascular geometry extracted from MRI TSE. (b) Frontal and top overview of temporal arachnoid cyst* [16].

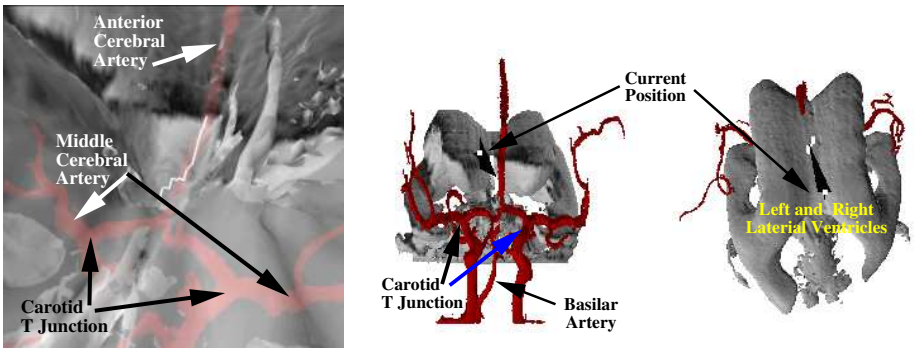


(a) (b)

**Figure 10:** *Ventriculostomy dataset: (a) Frontal view from the center of the lateral ventricles (first two ventricles); the septum between the lateral ventricles is dissolved. The white line marks the default camera path from the left lateral ventricle through the foramen of Monro into the third ventricle. (b) Frontal and top overview of ventricular system*[16].

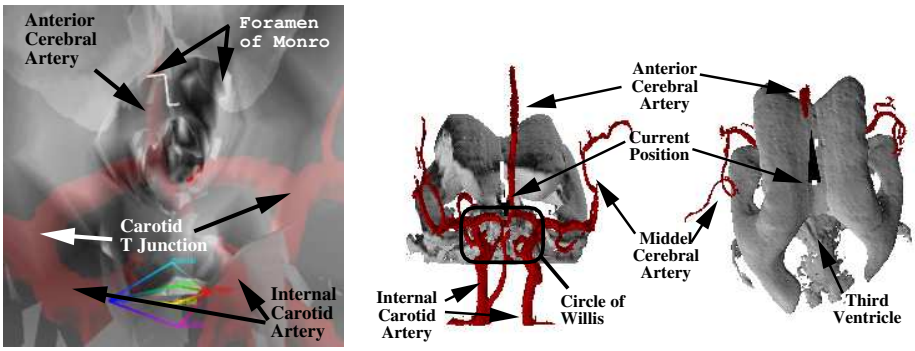


(a) (b)

**Figure 11:** *Ventriculostomy dataset: (a) Frontal view from the cerebral aqueduct entrance in the third ventricle. The floor of the third ventricle – the potential location for a new CSF drain – is bounded by the arterial* circle of Willis*, a potential cause for mass bleeding. (b) Frontal and top overview of ventricular system*[16].

vascular systems are mainly performed using Maximum-Intensity-Projections (MIP) or slicing through the 3D dataset. In contrast, using virtual endovascular methods (virtual endoscopy) enables both quantitative and qualitative analysis of the blood vessels[27].

After a segmentation and classification operation, the visual reconstruction of the blood vessels in the scanned area can be generated from the volume data. However, due to venous reflux of the contrast agent (if used), occasionally more blood vessels of the respective area are selected than the vessels of interest. This can lead to a situation where the important information is hidden behind less important information. Two techniques are applied to solve this situation. The application of virtual clips limits the segmentation of the vessel tree to the part of the vessels the physician is interested in[84, 17]. The second technique applies methods from virtual endoscopy[13, 17, 14] to generate an interactive environment for the vascular examination from a point of view which is inside the vessels.

### 5.4.2. Angioscopy of Cerebral Blood Vessels

A common procedure in neuroradiology is the examination of extra- and intracranial blood vessels. The major motivation behind these examinations is the diagnosis of cerebral aneurysms. Clinically, two major forms of aneurysms are distinguished; the *fusiform aneurysm* and the *non-fusiform* or *other aneurysms*. The fusiform aneurysm is an expansion of an arterial blood vessel through all of its wall layers (see Fig. 12a). The basic criterion is that no *neck of the aneurysm* can be determined which renders the aneurysm effectively as non-treatable. In contrast, a neck or exit can be identified for *non-fusiform aneurysm* (see Fig. 12b). From an anatomic point of view, other distinctions are possible according to the shape and location of the aneurysms. Furthermore, some aneurysms include a rupture of the inner arterial wall layers, the intima and media. The remaining adventitia layer forms a saccular deformation which is very sensitive to pressure. However, these differences cannot be easily identified which results in no clinical relevance of this distinction.

The expansion of the aneurysms can introduce pressure on other blood vessels – possibly resulting in the occlusion of that blood vessel –, or on surrounding commissures (nerve fibers). This pressure can result in severe headache, partial paralysis, or a stroke. Furthermore, strong blood flow vortices and swirls at the neck and in the aneurysms increase the risk of a highly dangerous rupture of the artery, in particular if the blood pressure is increasing due to physical exercises. This rupture in turn results in the serious destruction or necrosis of the surround brain tissue or in a lethal mass bleeding.

The usual procedures to treat aneurysms include neurosurgical and neuroradiological interventions. The major neurosurgical procedure is the exclusion of the aneurysm from the blood flow by positioning a clip on the neck of the aneurysm.

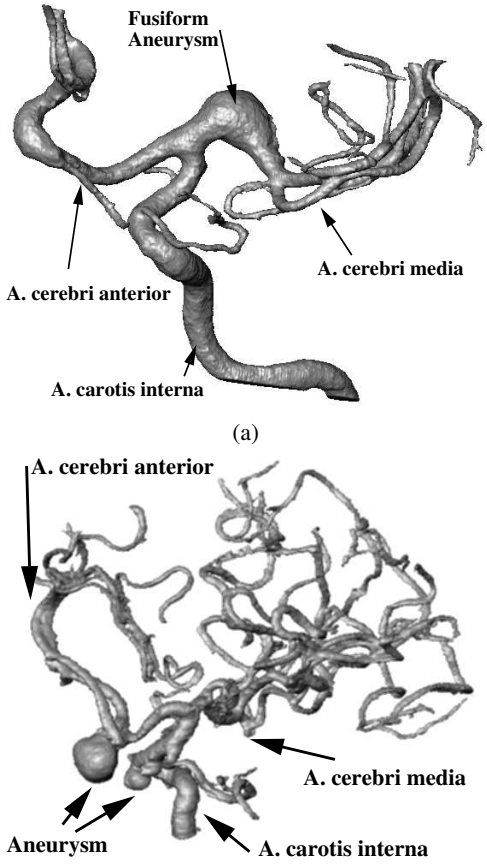


**Figure 12:** *Cerebral aneurysms; (a) fusiform aneurysm, (b) non-fusiform aneurysm.*

In neuroradiology, tiny platinum spirals ("coils") are introduced into the dome of the aneurysm using a micro-catheter, which is usually inserted via one of the femoral arteries of the legs. Together with the clotting of the thrombocytes, the coils close the aneurysm from the blood stream. All these interventions require the identification of the neck and exit of the aneurysms. However, these tasks can frequently not be achieved with standard 2D angiographies, MIPs, or slicing through the volume dataset. 3D geometry reconstructions using direct or indirect volume rendering techniques[12] have been recently introduced into the clinical practice of research hospitals[39] to provide a better understanding of the angioarchitecture of aneurysms in complex blood vessel trees. In particular endovascular inspections of the blood vessel can provide valuable information on the position, orientation, and connection of the aneurysm [53].

We applied the VIVENDI framework for the endovascular identification of the neck, exit, and dome of cerebral aneurysms[17]. The geometry representing the inner surface

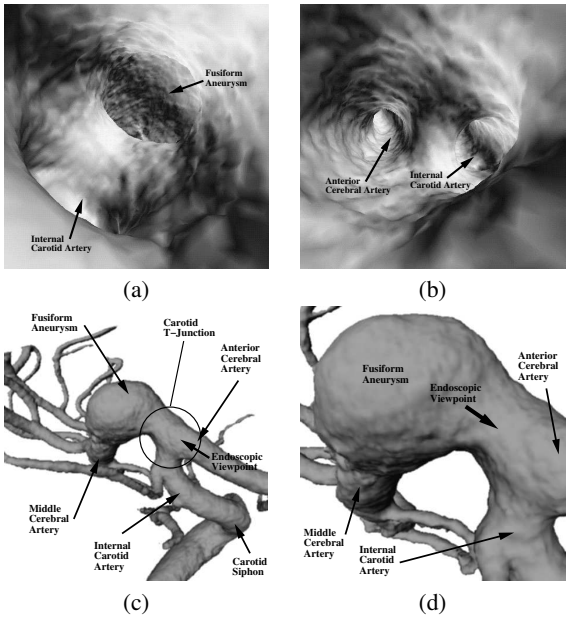


**Figure 13:** *Patient One – (a) Fusiform aneurysm of the middle cerebral artery. (b ) Carotid T-junction as seen from the middle cerebral artery. (c) and (d) show magnifications of views on the aneurysm from outside of the blood vessels. The respective view-points of (a), (b) are annotated in (c) and (d).*

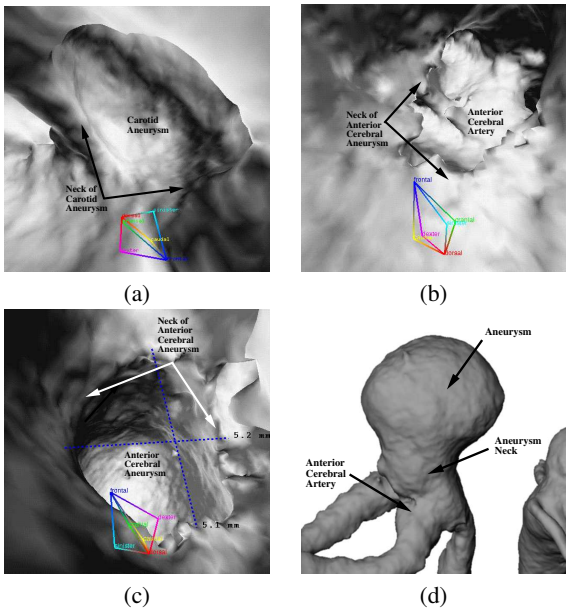


**Figure 14:** *Patient Two – (a) Exit of carotid aneurysm. (b) View from anterior cerebral aneurysm into anterior cerebral artery. (c) View from anterior cerebral artery into aneurysm. Measurements show the size of the aneurysm neck. (d) Anterior cerebral artery from outside.*

of the blood vessels is reconstructed using data from rotational angiography, which provides an isotropic volume dataset at a very high resolution with a voxel spacing in the sub-millimeter range.

The first patient dataset shows a fusiform aneurysm of the middle cerebral artery (see Fig. 12a). It is located close to the carotid T-junction, where the internal carotid artery branches into the anterior and middle cerebral arteries. Figure 13a shows the exit (entrance) of the fusiform aneurysm as seen from the anterior cerebral artery at the T-junction. Below is the entrance of the internal carotid artery. An endovascular view from the middle cerebral artery to the T-junction can be seen in Figure 13b. To the left is the entrance to the frontal anterior cerebral artery, to the right is the entrance to the internal carotid artery. In Figure 13c and d, magnifications of the aneurysm from view-points outside of the blood vessels can be seen. Unfortunately, the fusiform nature of the aneurysm does not permit an effective treatment.

The second patient has several non-fusiform aneurysms; an aneurysm of the internal carotid artery (see Fig. 12b right) and an aneurysm of the anterior cerebral artery (see Fig. 12b left and Fig. 14d). Figure 14a shows the exit (entrance) of the carotid aneurysm. The neck is easily identified from the endovascular view. Similar, Figure 14c shows the neck of the anterior cerebral aneurysm. Measurements suggest that the approximate radius of the aneurysm's head is 5mm. Figure 14b shows the respective view from inside of the aneurysm to the anterior cerebral artery. Finally, Figure 14d shows the aneurysm from an outside view. The visualizations of the anterior cerebral aneurysm show that all three branches of the anterior cerebral artery are closely located to the aneurysm. However, clipping allows the exclusion of the aneurysm without occluding one of these branches. This result was confirmed by the neurosurgical examination and treatment which applied a clip to the anterior aneurysm. The smaller carotid aneurysm was coiled during a successful interventional neuroradiologic procedure.

### 5.4.3. Angioscopy of Coronary Blood Vessels

The heart of the human body is responsible for circulating the blood through the blood vessels of the human body. It is organized into four chambers, the atria and ventricles of the heart (see Fig. 15). One atrium and one ventricles belong to the *right heart*, or *left heart* respectively. The heart is connected with the blood vessel system through veins (leading towards the heart) and arteries (leading away from the heart). The venous blood from the various body parts arrives in the *right atrium* through the *great veins*, the *superior* and *inferior vena cava*. It enters through the right *atrioventricular valve*, the *tricuspid valve*, into the *right ventricle*, where it is pumped via the *pulmonary valve* into the *pulmonary artery* to the lungs. After the refreshing of the blood with

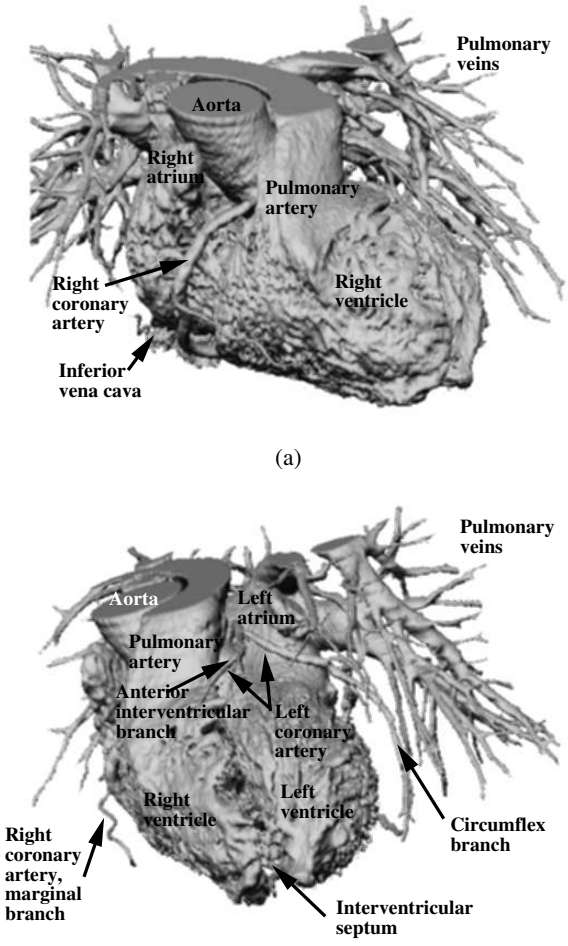


**Figure 15:** *Contrast media filled cavities of the heart: (a) Front/top view, (b) left/top view*[11].

oxygen in the lungs, it arrives through the *pulmonary veins* in the left atrium. It passed via the *left atrioventricular valve*, the *mitral valve*, into the *left ventricle* and is pumped via the *aortic valve* into the *aorta*, which distributes the blood to all body parts. Directly after the aortic valve are the entrances to the *left* and *right coronary arteries*, which supply the heart muscle with blood. The left coronary artery bifurcates into the *anterior interventricular branch* and the *circumflex branch*, which supplies most of the left heart, and it is the main source of supply of the interventricular septum – which separates the left and right ventricles –, that includes most of the conducting system of the heart. The right coronary artery extends over the right heart. It supplies this part of the heart, the interatrial septum – which separates the left and right atria –, and additionally the interventricular septum, including the sinuatrial and atrioventricular nodes, which are the major parts of the conduction system of the heart [43].

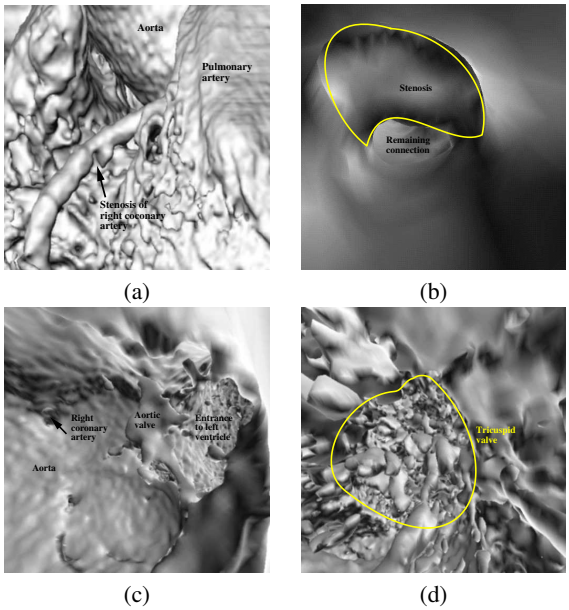


**Figure 16:** *Virtual endoscopy of the heart: (a) Outside reconstruction of stenosis of right coronary artery; (b) endoscopic view on stenosis; (c) view from aorta onto (remainder of) aortic valve; (d) view from right ventricle onto (remainder of) tricuspid valve* [11].

Cardiac diseases are among the number one causes of life-threatening diseases in Europe and North-America. Usually, the under-supply of the heart muscle with oxygen through the blood leads to severe arrhythmia. This arrhythmia can cause an electro-mechanic decoupling of the conduction of the heart, resulting in a dangerous reduction of the pumping performance, in a possible collapse of the blood circulation, and finally the death of the patient. Even if the arrhythmia is not leading to a fatal decoupling of the conduction, the missing supply of oxygen leads to the necrosis of that part of the heart muscle, if necessary medical procedure are not applied in time. The actual cause of the under-supply of the heart muscle is usually a stenosis or an occlusion of a coronary artery. Other reasons for arrhythmias are direct injuries of the heart muscle by force, failure of the valves of the heart, or infectious diseases.

For the diagnosis of these malfunctions, several clinical and laboratory tests are applied. For imaging, echo cardiography, coronary angiography, or nuclear medicine methods are used. However, only 3D scanning methods are able to generate volumetric data of the heart. Unfortunately, most modalities are too slow to avoid motion artifacts of the fast moving heart. More or less only ECG-triggered (Electro-Cardio-Gramme) spiral CT provides scanning which cap-

tures volumetric data of the heart that is widely motion artifact free. With the introduction of multi-slice CT, enough spatial resolution is also available for 3D coronary angiography.

Based on an anisotropic dataset from multi-slice CT coronary angiography, we explore the use of virtual endoscopy for virtual angioscopy of the heart[11]. The dataset consist of 150 slices at a slice distance of 1.25mm. Each of the slices has a resolution of $512 \times 512$ pixels at a pixel distance of 0.59 mm. Outside views on the reconstructed, contrast media filled cavities of the heart can be seen in Figure 15. The reconstructed geometry of the heart is very complex. From more than two million polygons, more than 80% of the geometry was culled by our visibility driven rendering, thus obtaining a frame-rate with an average of 4.2 fps on a typical path through the right heart. The low culling and frame-rate are a result of the deep visibility within the chambers of the heart which reduces possible culling benefits.

The coronary valves, which open and close at a high speed, cannot be reconstructed completely, due to motion artifacts in the scanned dataset (see Fig. 16c and d). In particular the right atrium of the heart is subject to artifacts which are due to the injection of the contrast agent and they can be seen in the respective slices of the CT dataset. However, other important features of the anatomy of the heart of the patient are visible, such as the aorta, the pulmonary artery, the great veins, the pulmonary veins, and the coronary arteries. Of special interest are the latter one's, since most of the cardiac emergencies result from a stenosis of these arteries. Figure 16a and b shows such a stenosis of the right coronary artery, which supplies the right heart and important parts of the conduction system of the heart. Measurements of the diameter of the blood vessel at of the stenosis provide a quantitative evaluation of the stenosis. Additionally, measurements of the volume of the ventricles provide information of the performance of the heart.

## 5.5. Virtual Bronchoscopy

### 5.5.1. Motivation

Among the most important organ systems of the human body are respiratory functions. They transports air into the body (inhaling) and removes exhausted air from the body during the exhale. The exchange of the air takes place in the lungs, which are a complementary system of airways and blood vessels. Both systems are supplied through large pipe-like structures which split successively into smaller ones, thus creating the tracheo-bronchial (airways) and blood vessel tree.

The tracheo-bronchial tree is connected to the outside through the trachea which splits into the main bronchi (left and right lungs) at the main bifurcation. The inhaled air is distributed through the bronchial tree down to the alveoli where the oxygen/carbon-dioxide exchange between air and blood takes place. The exhausted air (enriched with carbon-dioxide) is then transported back up to the trachea during the exhale. The tracheo-bronchial tree is complemented by a system of pulmonary venous and arterial blood vessels which transports the blood to and from the heart into the lungs.

Several pathologies can jeopardize a sufficient lung function. Among them are tumors, pulmonary embolism, collapse of the lungs (atelectasis), pneumonia, emphysema, asthma, and many more. For a proper diagnosis and treatment, the respective pathologies need to be identified and in some cases quantified. In the case of lung-surgery, this information is necessary for the intervention planning where the anatomical relation of diseased bronchi to non-diseased areas is required pre-operatively, ie. to provide a safe distance to essential structures and to determine resectability. However, the usage of virtual bronchoscopy as a diagnostic tool is limited, since detailed information on the mucosa is not available, thus tumors limited to that areas cannot be detected easily[65].

The current gold-standard to identify the respective lung parenchyma and airways is computed tomography (CT) that is performed prior to a bronchoscopy, a tool for inspections of the trachea and central bronchi and deriving tissue samples. Due to the recent technical development improving resolution and scan velocity, multi-slice CT – in connection with virtual bronchoscopy – became a promising alternative to bronchoscopy, if tissue samples are not required. This is amplified by the fact that optical bronchoscopy is limited by smaller, lower airways (third generation and up) or by obstructions. Nevertheless, even smaller structures of the lower airways are extremely difficult to segment from CT datasets, due to leakages, caused by the notorious partial volume effect and due to the lack of sufficient contrast to surrounding tissue or air. Mayer et al.[54] presented a segmentation approach that enables also the segmentation of small airways. Here, we concentrate on the virtual endoscopy of the airways, the virtual bronchoscopy to visualize airways, blood vessels, and tumors.

### 5.5.2. Methods for Virtual Bronchoscopy

Virtual bronchoscopy requires data of a high spatial and temporal resolution, since the structures of interest can be quite small. Furthermore, breathing artifacts can reduce the quality of the data. Therefore, we are using a multi-slice CT scanner to acquire approximately 250-300 images of $512 \times 512$ voxels of a sub-millimeter spacing. Based on these data and a provided segmentation of the airways, blood vessels, and possible tumors[54], we reconstruct a surface representation of the lungs.

After the segmentation, we explored a subset of the datasets interactively (more than 30fps on a standard PC[‡])

‡ In the full opaque mode, a Linux PC equipped with an P4 CPU

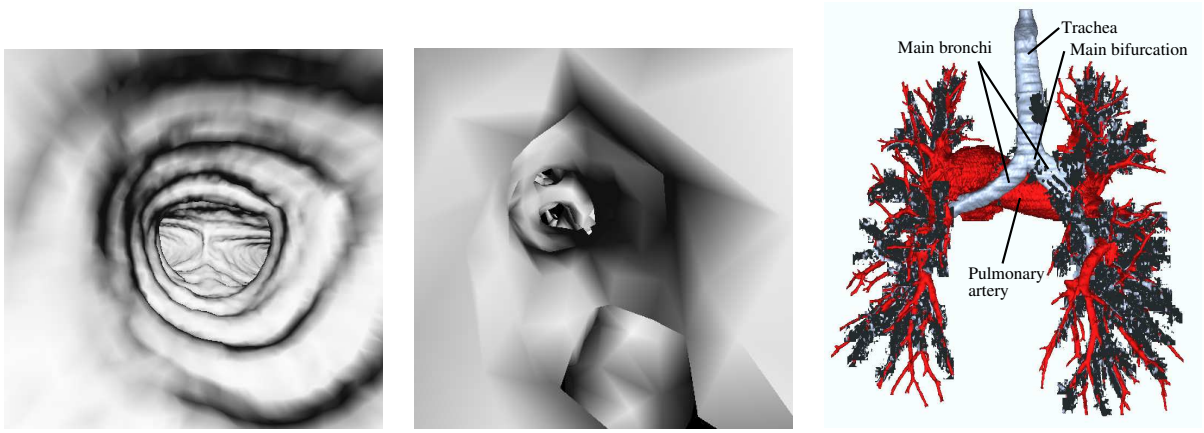


(a) (b) (c)

**Figure 17:** *Virtual endoscopy: (a) View in trachea down to main bi-furcation, (b) approximately the seventh generation of the lower airways, mainly segmented by 2D template matching. The diamond shape interpolation artifacts are due to high zoom factor in this close-up.(c) shows an annotated outside representation with the tracheo-bronchial tree (grey) and pulmonary arteries (red) from a view behind the patient body (left image side is left patient side).*

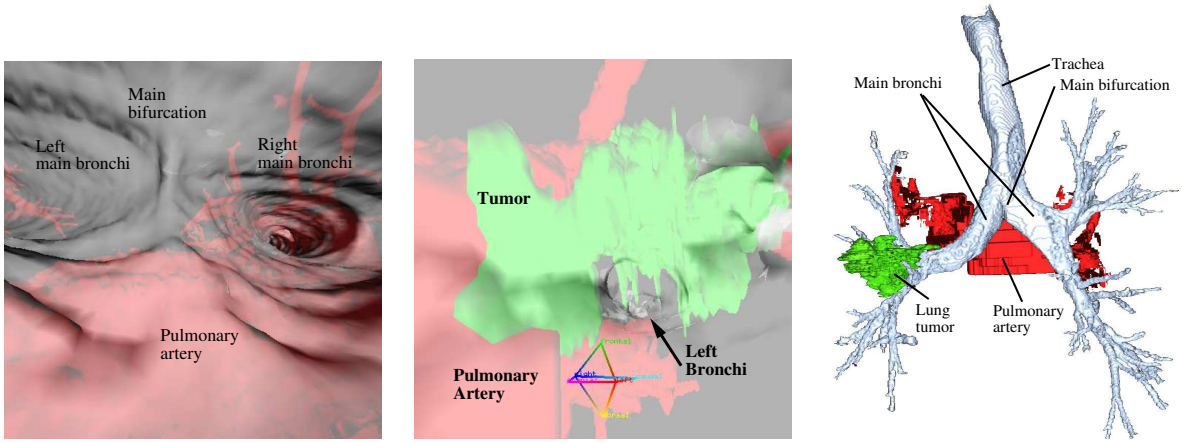


(a) (b) (c)

**Figure 18:** *Virtual endoscopy: (a) Semi-transparent rendering of view in trachea at main bi-furcation. The pulmonary arteries (red) are visible through the inner surface of the tracheo-bronchial tree (same dataset as in Fig 17). (b) shows the a similar situation further down the left bronchi. Straight ahead is a large tumor (green) of the left lungs, which eventually will obstruct the left bronchi (same dataset as in Fig. 18c). (c) shows an annotated outside representation of another dataset with the tracheo-bronchial tree (grey), pulmonary arteries (red), and a tumor (green) in the left lung (view from behind the patient).*

using the virtual endoscopy software[13]. The exploration exposed a high quality reconstruction, even of small structures throughout the dataset. In Figure 17, we show two snapshots from a regular virtual bronchoscopy. The left image (Fig. 17a) shows the endo-view from the trachea looking down to the main bifurcation, where the tracheo-bronchial tree splits into the left and right lungs. Figure 17b shows the limits of the currently possible segmentation; the virtual endoscope is located approximately in the seventh generation of the lower airways. Due to the high zoom-factors, the typical diamond-shape interpolation artifacts of trilinear interpolation on the voxel cell grid are exposed. Blood vessels were visualized to provide more context information (Fig. 17c).

In Figure 18, we show a more complex situations, where the surrounding arterial blood vessels are visible through the inner surface of the tracheo-bronchial tree. Figures 18b and c show a tumor in the left lung in green. At the same time, poor contrast and beam hardening artifacts of the voxels of the pulmonary arteries expose segmentation difficulties; the blood vessel tree is only incompletely segmented (Fig. 18c).

## 6. Discussion of Virtual Endoscopy

In Section 5, we presented several applications of virtual endoscopy. The different objectives of the applications impose specific requirements on the virtual endoscopy system. An educational objective focuses more on the visual quality that demonstrate the general topological and geometric aspects of the specific patient anatomy. In contrast, the accuracy of fine details is only of limited importance, if the details are not the subject of the examination. However, this is different for a clinical objective where the accurate rendering is one of the major factors that determine the usability, where an incorrectly represented blood vessel connection might have a fatal impact on the medical intervention. If virtual endoscopy is used for planning an intervention, it is important that relevant anatomical structures are represented appropriately, since otherwise the planned access path (ie., in virtual ventriculoscopy) might be occluded in the "real world" anatomy. Similar, the visual representation must be highly accurate for intra-operative navigation to provide usable information to the surgeon.

There are several sources of errors that can lead to an inaccurate visual representation of anatomical structures in virtual endoscopy. Most notorious are partial volume effects and undersampling which generate "fake" connections between the various caverns that are actually not connected. Furthermore, motion artifacts can reduce the visual quality severely or distort the actual anatomical geometry. These artifacts are generated by movement of the patient during a (long) medical scanning procedure. Another example is scanning of fast moving body parts, ie., the valves of the heart, which cannot be traced by modern volumetric scanners.

Even if these effects do not reduce the accuracy of the volumetric representation, the quality of the visualization depends heavily on the quality of the segmentation process. Isovalues that are not selected with sufficient particularity lead to holes in surfaces, if the isovalue is to low, or existing holes in the surface are closed and vice versa. In Figure 19, the hole in the ventricular septum between the two lateral ventricles varies in size, depending on the isovalue. However, the question of which isovalue is correct is not easy to answer in this case, because the volume data in that area is inconclusive (Fig. 19c); due to partial volume effects, it is not clear exactly what size the hole is. In [10], I provide a more detailed discussion the various sources of artifacts.

Besides visual quality, interactivity is a major issue for virtual endoscopy. A rendering speed significantly below interactive rendering (10 fps) is usually not well accepted in the medical community. If virtual endoscopy is used for inter- operative navigation, no measurable rendering lag is acceptable. The virtual endoscopy system must deliver real-time rendering performance to represent the geometry of the current view of the endoscope immediately with every movement of the endoscope. These requirements are usually not met with most virtual endoscopy systems. Even the VIVENDI system does not provide sufficient performance for all applications; virtual angioscopy of the heart provides only a few frames per second. The widely visible inner geometry of the left and right ventricles of the heart allows only a culling rate of 80%, which leaves a high polygonal complexity for rendering. For all other applications however, VIVENDI meets the requirements for interactive exploration and in particular for inter-operative real-time navigation of ventricular MRI datasets.

### Virtual Endoscopy versus Optical Endoscopy

The more general question of whether virtual endoscopy provides more scientific or medical insights, more patient safety or comfort, or an economic benefit is more difficult to answer. As for most scientific problems, the answer depends on the actual goal of the procedure, the qualities of alternative medical procedures, and various costs of the procedures.

In all procedures that require a histological examination of a tissue sample under a microscope, virtual endoscopy is not able to compete. The data resolution of modern 3D scanners does not reach into the resolution of a microscope, although it is already in a sub-millimeter range for rotational angiography. Furthermore, texture information, such as structure, color, and reflections is also not captured by 3D scanners.

running at 2.8GHz and an ATI Radeon 9700Pro graphics accelerator rendered more than 1.1M triangles (tracheo-bronchial tree is visible only) at 53fps. In the semi-transparent mode, it achieved 36fps rendering the tracheo-bronchial and the pulmonary artery trees of almost 2M triangles. All geometry is arranged in triangle strips, compiled in OpenGL display lists.


(a) (b) (c)

**Figure 19:** *Hole of different sizes in ventricular septum (of the brain); isovalue in (a) is lower than in (b). (c) shows a slice from the original volumetric data of that area.*

All applications that heavily depend on this information will not succeed with virtual endoscopy. Similarly, if the medical procedure includes the removal of tissue (ie., lesions or tumors), or other objects, invasive or minimally invasive procedures cannot be replaced by virtual endoscopy, since it does not interact with the actual body of a patient.

However, if the relevant information can be represented as geometric shape – ie., a polyp of virtual colonoscopy –, virtual endoscopy can be used for diagnostic purposes. Furthermore, it provides insights into body parts that might not be accessible to current medical procedures. The virtual representation based on scanner data provides access to virtually all scan-able body parts. Physical limitations of optical endoscopes – ie., the limited flexibility and navigation of the endoscope used for ventriculoscopy, the insuperable obstruction of folds in a colon for optical colonoscopy – are not shared with virtual endoscopes. Similarly, virtual endoscopes do not share the frequent unpleasantness of optical endoscopes. The patient interaction is limited to the scanning procedure, and is therefore providing much more patient comfort and acceptance. In addition, data acquisition and the actual virtual procedure are not necessarily at the same location. This geographical decoupling allows tele-medical procedures, which are not possible with optical endoscopy, where data acquisition and procedure are inseparably combined.

From an economic point of view, virtual endoscopy does produce fewer costs than the optical or conventional counterpart, since usually no sedation, patient preparation, or even hospitalization is required. The necessary computational expenses can be seen as additional post-processing of the volume reconstruction of the scanner. However, procedures, which combine virtual and optical methods, ie., ventriculoscopy, do not benefit from these costs; the goal of this combination was to reduce the risk of complications and to increase the success of the intervention.

A study on the accuracy of virtual colonoscopy compared to conventional colonoscopy has been presented by Fenlon et al.[33]. The authors found that the performance of virtual colonoscopy is comparable to optical, as long as the data resolution is sufficient to detect polyps of the respective size. Only polyps with a size close to the sampling rate were not as easy detectable as larger ones. Problems arose also from residual stool, which often was the cause of a false positive finding. Techniques like digital cleansing in the acquired datasets[49] might help to reduce the number of these false positives.

## 7. Conclusions

In the report, we have discussed several virtual endoscopy systems that are used in research and clinical environments. These systems address different objectives and are using henceforth different rendering techniques and adopt different camera navigation paradigms.

I also presented several applications of virtual endoscopy in the clinical practice. While some of these applications aim at support for "traditional" interventions, some try to replace their real world counterpart, ie., colonoscopy. However, it still remains to be shown in most applications that virtual endoscopy actually provides an added value, a fact that holds for most advanced medical imaging techniques.

### Finally....

Time flies, a fact of life that is also true for publications. Since the writing of the State-of-the-art-report, my notes have probably improved with more material and – hopefully only minor – corrections. The updated version – along with the slides – will be available through my webpage at: http://www.gris.uni-tuebingen.de/~bartz/tutorials

**Acknowledgements**

This work has been supported by the German Federal Ministry of Research and Education, by the State of Baden-Württemberg, by the Hewlett-Packard Corporation, by DFG project CatTrain, and by the Competence Center of minimally invasive medical technology Tübingen-Tuttlingen.

I like to thank my collaborators in the many projects, namely Özlem Gürvit, now with the University Hospital of Marburg, Dirk Freudenstein, Jürgen Hoffmann, Dirk Troitsch, Martin Skalej, Ludger Schnieder, Florian Dammann, Andreas Bode, Andreas Kopp, and Claus Claussen of the University Hospital Tübingen, and Dirk Mayer of the University Hospital Mainz. Furthermore, I like to thank the members of the VCM group in Tübingen: Anxo del Río, Jan Fischer, Jasmina Orman, and Zein Salah.

**References**

1. J. Airey, J. Rohlf, and F. Brooks. Towards Image Realism with Interactive Update Rates in Complex Virtual Building Environments. In *Proc. of ACM Symposium on Interactive 3D Graphics*, pages 41–50, 1990. 6
2. D. Auer and L. Auer. Virtual Endoscopy - A New Tool for Teaching and Training in Neuroimaging. *International Journal of Neuroradiology*, 4:3–14, 1998. 3, 4
3. L. Auer, D. Auer, and J. Knoplioch. Virtual Endoscopy for Planning and Simulation of Minimally Invasive Neurosurgery. In *First Joint Conference, Computer Vision, Virtual Reality and Robotics in Medicine and Medical Robotics and Computer-Assisted Surgery*, volume LNCS 1205, pages 315–318, 1997. 4, 5
4. A. Vilanova Bartrolí. *Visualization Techniques for Virtual Endoscopy*. PhD thesis, Technical University of Vienna, 2001. 7
5. A. Vilanova Bartrolí, A. König, and E. Gröller. VirEn: Virtual Endoscopy System. *Machine Graphics & Vision*, 8(3):469–487, 1999. 3, 4, 5, 7
6. A. Vilanova Bartrolí, R. Wegenkittl, A. König, and E. Gröller. Nonlinear Virtual Colon Unfolding. In *Proc. of IEEE Visualization*, 2001. 4, 8
7. A. Vilanova Bartrolí, R. Wegenkittl, A. König, and E. Gröller. Perspective Projection Through Parallely Projected Slabs For Virtual Endoscopz. In *Proc. of Spring Conference on Computer Graphics*, pages 287–295, 2001. 8
8. A. Vilanova Bartrolí, R. Wegenkittl, A. König, E. Gröller, and E. Sorantin. Virtual Colon Flattening. In *Data Visualization (Proc. of Symposium on Visualization)*, pages 127–136, 2001. 4, 8
9. D. Bartz. Prototyping a Virtual Colonoscopy System. Master's thesis, Dept. of Computer Science, University of Erlangen-Nürnberg, 1996. 6, 9
10. D. Bartz. Möglichkeiten und Grenzen der virtuellen Endoskopie. In *Proc. of Simulation und Visualisierung*, 2003. 3, 21
11. D. Bartz, Ö. Gürvit, M. Lanzendörfer, A. Kopp, A. Küttner, and W. Straßer. Virtual Endoscopy for Cardio Vascular Exploration. In *Proc. of Computer Assisted Radiology and Surgery*, pages 960–964, 2001. 3, 18, 19
12. D. Bartz and M. Meißner. Voxels versus Polygons: A Comparative Approach for Volume Graphics. In *Proc. of Volume Graphics*, pages 33–48, 1999. 16
13. D. Bartz and M. Skalej. VIVENDI - A Virtual Ventricle Endoscopy System for Virtual Medicine. In *Data Visualization (Proc. of Symposium on Visualization)*, pages 155–166,324, 1999. 2, 3, 4, 5, 7, 9, 11, 13, 16, 21
14. D. Bartz, M. Skalej, D. Welte, and W. Straßer. 3D Interactive Virtual Angiography. In *Proc. of Computer Assisted Radiology and Surgery*, pages 44–48, 1999. 16
15. D. Bartz, M. Skalej, D. Welte, W. Straßer, and F. Duffner. A Virtual Endoscopy System for the Planning of Endoscopic Interventions in the Ventricle System of the Human Brain. In *Proc. of BiOS'99: Biomedical Diagnostics, Guidance and Surgical Assist Systems*, volume 3514, pages 91–100, 1999. 3, 11, 12
16. D. Bartz, W. Straßer, Ö. Gürvit, D. Freudenstein, and M. Skalej. Interactive and Multi-modal Visualization for Neuroendoscopic Interventions. In *Data Visualization (Proc. of Symposium on Visualization)*, pages 157–164, 2001. 3, 13, 15
17. D. Bartz, W. Straßer, M. Skalej, and D. Welte. Interactive Exploration of Extra- and Intracranial Blood Vessels. In *Proc. of IEEE Visualization*, pages 389–392,547, 1999. 3, 4, 13, 16
18. J. Beier, T. Diebold, H. Vehse, G. Biamino, E. Fleck, and R. Felix. Virtual Endoscopy in the Assessment of Implanted Aortic Stents. In *Proc. of Computer Assisted Radiology*, pages 183–188, 1997. 3, 4
19. I. Bitter, M. Sat, M. Bender, K. McDonnell, A. Kaufman, and M. Wan. CEASAR: A Smooth, Accurate and Robust Centerline Extraction Algorithm. In *Proc. of IEEE Visualization*, pages 45–52, 2000. 6
20. A. Bode, F. Dammann, E. Pelikan, M. Heuschmid, E. Schwaderer, M. Schaich, and C. Claussen. Analyse von Artefakten bei der virtuellen endoskopischen Darstellung auf Basis von Spiral-CT-Daten. *RöFö: Fortschritte auf dem Gebiet der Röntgenstrahlen und der neuen bildgebenden Verfahren*, 173:245–252, 2001. 3, 4
21. B. Cabral, N. Cam, and J. Foran. Accelerated Volume Rendering and Tomographic Reconstruction Using Texture Mapping Hardware. In *Proc. of Symposium on Volume Visualization*, pages 91–98, 1994. 7

22. S. Chen. Quicktime VR – An Image-based Approach to Virtual Environment Navigation. In *Proc. of ACM SIGGRAPH*, pages 29–38, 1995. 4, 8

23. Z. Cho, J. Jones, and M. Singh. *Foundations of Medical Imaging*. John Wiley, New York, NY, 1993. 14

24. L. Cohen, P. Basuk, and J. Waye. *Practical Flexible Sigmoidoscopy*. Igaku-Shoin, New York, NY, 1995. 9

25. T. Cullip and U. Neumann. Accelerating Volume Reconstruction with 3D Texture Hardware. Technical Report TR93-027, University of North Carolina at Chapel Hill, 1993. 2, 5, 6, 7

26. F. Dachille, K. Kreeger, M. Wax, A. Kaufman, and Z.Liang. . In *Proc. of SPIE Medical Imaging*, 2001. 3

27. C. Davis, M. Ladds, B. Romanowski, S. Wildermuth, J. Knoplioch, and J. Debatin. Human Aorta: Preliminary Results with Virtual Endoscopy Based on Three-dimensional MR Imaging Data Sets. *Radiology*, 199:37–40, 1996. 3, 4, 5, 16

28. E. Dijkstra. A Note on Two Problems in Connection with Graphs. *Numerische Mathematik*, 1:269–270, 1959. 6

29. F. Duffner, W. Dauber, M. Skalej, and E. Grote. A New Endoscopic Tool for the CRW Stereotactic System. In *Stereotactic and Functional Neurosurgery*, volume 67(3-4), pages 213–217, 1994. 1, 11

30. K. Engel. Interactive High-Quality Volume Rendering with Flexible Consumer Graphics Hardware. In *Eurographics State-of-the-Art-Report S2*, 2002. 3

31. K. Engel, M. Kraus, and T. Ertl. igh-Quality Pre-Integrated Volume Rendering Using Hardware-Accelerated Pix. In *Proc. of Eurographics/SIGGRAPH Workshop on Graphics Hardware*, pages 9–16, 2001. 2

32. R. Fahrig. *Computed Rotational Angiography*. PhD thesis, University of Western Ontario, 1999. 14

33. H. Fenlon, D. Nunes, P. Schroy, M. Barish, P. Clarke, and J. Ferrucci. A Comparison of Virtual and Conventional Colonoscopy for the Detection of Colorectal Polyps. *New England Journal of Medicine*, 341(20):1496–1503, 1999. 9, 22

34. G. Ferretti, D. Vining, J. Knoplioch, and M. Coulomb. Tracheobronchial Tree: Three-Dimensional Spiral CT with Bronchoscopic Perspective. *Journal of Computer Assisted Tomography*, 20(5):777–781, 1996. 3, 4

35. D. Freudenstein, D. Bartz, M. Skalej, and F. Duffner. A New Virtual System for Planning of Neuroendoscopic Interventions. *Computer Aided Surgery*, 6(2):77–84, 2001. 1

36. T. Galyean. Guided Navigation of Virtual Environments. In *Proc. of ACM Symposium on Interactive 3D Graphics*, pages 103–104, 1995. 3, 4, 6

37. D. Gering, A. Nabavi, R. Kikinis, N. Hata, L. O'Donnell, E. Grimson, F. Jolesz, P. Black, and W. Well. An Integrated Visualization System For Surgical Planning and Guidance Ising Image Fusion and Open MR. *Journal on Magnetic Resonance Imaging*, 13:967–975, 2001. 4, 8

38. E. Gobbetti, P. Pili, A. Zorcolo, and M. Tuveri. Interactive Virtual Angioscopy. In *Proc. of IEEE Visualization*, pages 435–438, 1998. 3, 4, 6, 7

39. Ö. Gürvit, M. Skalej, R. Riekmann, U. Ernemann, and K. Voigt. Rotational Angiography and 3D Reconstruction in Neuroradiology. *electro medica*, 68(1):31–37, 2000. 14, 16

40. S. Haker, A. Tannenbaum, and R. Kikinis. Nondistorting Flattening Maps and 3D Visualization of Colon CT Images. *IEEE Transactions on Medical Imaging*, 19:665–670, 2000. 4

41. T. He and L. Hong. Reliable Navigation for Virtual Endoscopy. In *Proc. of IEEE Medical Imaging*, 1999. 3, 4

42. R. Hietala and J. Oikarinen. A Visibility Determination Algorithm for Interactive Virtual Endoscopy. In *Proc. of IEEE Visualization*, pages 29–36, 2000. 4

43. W. Hollinshead and C. Rosse. *Textbook of Anatomy*. Harper & Row, Publishers, Philadelphia, USA, 4th edition, 1985. 18

44. L. Hong, A. Kaufman, Y. Wei, A. Viswambharan, M. Wax, and Z. Liang. 3D Virtual Colonoscopy. In *Proc. of IEEE Symposium on Biomedical Visualization*, pages 26–32, 1995. 4, 6, 7

45. L. Hong, S. Muraki, A. Kaufman, D. Bartz, and T. He. Virtual Voyage: Interactive Navigation in the Human Colon. In *Proc. of ACM SIGGRAPH*, pages 27–34, 1997. 2, 3, 4, 5, 6, 7, 8, 9, 10

46. J. Kniss, K. Engel, M. Hadwiger, and C. Rezk-Salama. High Quality Volume Graphics on Consumer PC Hardware. In *ACM SIGGRAPH course 42*, 2002. 3

47. P. Lacroute and M. Levoy. Fast Volume Rendering Using a Shear-Warp Factorization of the Viewing Transformation. In *Proc. of ACM SIGGRAPH*, pages 451–458, 1994. 2

48. A. Laghi, P. Pavone, V. Panebianco, I. Carbone, and L. Francone. Volume-rendered Virtual Colonoscopy: Preliminary Clinical Experience. In *Proc. of Computer Assisted Radiology and Surgery*, pages 171–175, 1999. 3

49. S. Lakare, M. Wan, M. Sato, and A. Kaufman. 3d digi-

tal cleansing using segmentation rays. In *Proc. of IEEE Visualization*, pages 37–44, 2000. 22

50. W. Li and A. Kaufman. Real-Time Volume Rendering for Virtual Colonoscopy. In *Proc. of Volume Graphics*, 2001. 6

51. W. Lorensen and H. Cline. Marching Cubes: A High Resolution 3D Surface Construction Algorithm. In *Proc. of ACM SIGGRAPH*, pages 163–169, 1987. 2, 3, 5, 6, 7

52. W. Lorensen, F. Jolesz, and R. Kikinis. The Exploration of Cross-Sectional Data with a Virtual Endoscope. In R. Satava and K. Morgan, editors, *Interactive Technology and New Medical Paradigms for Health Care*, pages 221–230. 1995. 3, 4

53. B. Marro, D. Galanaud, C. Valery, A. Zouaoui, A. Biondi, A. Casasco, M. Sahel, and C. Marsault. Intracranial Aneurysm: Inner View and Neck Identification with CT Angiography Virtual Endoscopy. *Journal of Computer Assisted Tomography*, 21(4):587–589, 1997. 16

54. D. Mayer, D. Bartz, S. Ley, S. Thust, C. Heussel, H. Kauczor, and W. Straßer. Segmentation and Virtual Exploration of Tracheo-Bronchial Trees. In *Proc. of Computer Assisted Radiology and Surgery*, 2003. 3, 19

55. M. Meißner and S. Guthe. Interactive Lighting Models and Pre-Integration for Volume Rendering on PC Graphics Accelerators. In *Proc. of Graphics Interface*, 2002. 2

56. M. Meißner, U. Hoffman, and W. Straßer. Enabling Classification and Shading for 3D Texture Mapping Based Volume Rendering. In *Proc. of IEEE Visualization*, pages 207–214, 1999. 2

57. M. Meißner, J. Huang, D. Bartz, K. Müller, and R. Crawfis. A Practical Evaluation of Four Popular Volume Rendering Algorithms. In *Proc. of Symposium on Volume Visualization and Graphics*, pages 81–90, 2000. 2

58. C. Morosi, G. Ballardini, and P. Pisani. Diagnostic Accuracy of the Double-Contrast Enema for Colonic Polyps in Patients with or without Diverticular Disease. *Gastrointestinal Radiology*, 16:346–347, 1991. 9

59. K. Mueller and R. Crawfis. Elminating Popping Artifacts in Sheet Buffer-Based Splatting. In *Proc. of IEEE Visualization*, pages 239–246, 1998. 2

60. D. Nain, S. Haker, R. Kikinis, and W. Grimson. An Interactive Virtual Endoscopy Tool. In *Proc. of Workshop on Interactive Medical Image Visualization and Analysis*, 2001. 3, 4, 8

61. K. Novins, F. Sillion, and D. Greenberg. An Efficient Method for Volume Rendering using Perspective Projection. In *Proc. of ACM SIGGRAPH*, pages 95–102, 1990. 2

62. H. Pfister, J. Hardenbergh, J. Knittel, H. Lauer, and L. Seiler. The VolumePro Real-Time Ray-Casting System. In *Proc. of ACM SIGGRAPH*, pages 251–260, 1999. 8

63. J. Rodenwaldt, L. Kopka, R. Roedel, A. Margas, and E. Grabbe. 3D Virtual Endoscopy of the Upper Airways: Optimization of the Scan Parameters in a Cadaver Phantom and Clinical Assessment. *Journal of Computer Assisted Tomography*, 21(3):405–411, 1997. 3

64. S. Roettger, S. Guthe, D. Weiskopf, T. Ertl, and W. Strasser. Smart Hardware-Accelerated Volume Rendering. In *Data Visualization (Proc. of Symposium on Visualization)*, 2003. 2

65. P. Rogalla. Virtual Endoscopy: An Application Snapshot. *Medica Mundi*, 43(1):17–23, 1999. 3, 4, 19

66. P. Rogalla, A. Nischwitz, A. Heitema, R. Kaschke, and B. Hamm. Virtual Endoscopy of the Nose and the Paranasal Sinus. *European Radiology*, 16:787–789, 1998. 3

67. P. Rogalla, J. Terwissa van Scheltinga, and B. Hamm. *Virtual Endoscopy and Related 3D Techniques*. Springer-Verlag, Heidelberg, 2000. 3

68. J. Rohen. *Topographische Anatomie*. Schattauer Verlag, Stuttgart, Germany, 8th edition, 1987. 11

69. G. Rubin, C. Beaulieu, V. Argiro, H. Ringl, A. Norbash, J. Feller, M. Dake, R. Jeffrey, and S. Napel. Perspective Volume Rendering of CT and MR Images: Application for Endoscopic Imaging. In *Radiology*, volume 199, pages 321–330, 1996. 4, 5

70. T. Saito and J. Toriwaki. New Algorithms for Euclidian Distance Transformation of an N-Dimensional Digitized Picture with Applications. *Pattern Recognition*, 27(11):1551–1565, 1994. 6

71. W. Schroeder, K. Martin, and B. Lorensen. *The Visualization Toolkit*. Prentice Hall, Upper Saddle River, NJ, 2nd edition, 1998. 8

72. I. Serlie, F. Vos, R. van Gelder, J. Stoker, R. Truyen, F. Gerritsen, Y. Nio, and F. Post. Improved Visualization in Virtual Colonoscopy Using Image-based Rendering. In *Data Visualization (Proc. of Symposium on Visualization)*, pages 137–146, 2001. 4, 8

73. R. Shadidi, V. Argiro, S. Napel, L. Gray, H. McAdams, G. Rubin, C. Beaulieu, R. Jeffrey, and A. Johnson. Assessment of Several Virtual Endoscopy Techniques Using Computed Tomography and Perspective Volume Rendering. In *Proc. of Visualization in Biomedical*

*Computing*, volume LNCS 1131, pages 521–528, 1996. 4, 5

74. P. Strauss and Carey R. An Object-oriented 3D Graphics Toolkit. In *Proc. of ACM SIGGRAPH*, pages 341–349, 1992. 5

75. J. Sweeney and K. Müller. Shear-Warp Deluxe: The Shear-Warp Algorithm Revisited. In *Data Visualization (Proc. of Symposium on Visualization)*, pages 95–104, 2002. 2

76. D. Vining, R. Shifrin, E. Grishaw, K. Liu, and R. Choplin. Virtual Colonoscopy (abstract). In *Radiology*, volume 193(P), page 446, 1994. 3, 4, 9

77. D. Vining, R. Shifrin, E. Haponik, K. Liu, and R. Choplin. Virtual Bronchoscopy (abstract). In *Radiology*, volume 193(P), page 261, 1994. 3

78. D. Vining, D. Stelts, D. Ahn, P. Hemler, Y. Ge, G. Hunt, C. Siege, D. McCorquodale, M. Sarojak, and G. Ferretti. FreeFlight: A Virtual Endoscopy System. In *First Joint Conference, Computer Vision, Virtual Reality and Robotics in Medicine and Medical Robotics and Computer-Assisted Surgery*, volume LNCS 1205, pages 413–416, 1997. 3, 4, 5

79. M. Wan, F. Dachille, and A. Kaufman. Distance field based skeletons for virtual navigation. In *Proc. of IEEE Visualization*, pages 239–246, 2001. 6, 7

80. M. Wan, A. Kaufman, and S. Bryson. High-performance presence-accelerated ray casting. In *Proc. of IEEE Visualization*, pages 379–388, 1999. 4

81. M. Wan, A. Sadig, and A. Kaufman. Fast and reliable space leaping for interactive volume rendering. In *Proc. of IEEE Visualization*, pages 195–202, 2002. 6

82. M. Wan, Q. Tang, A. Kaufman, Z. Liang, and M. Wax. Volume Rendering Based Interactive Navigation within the Human Colon. In *Proc. of IEEE Visualization*, pages 397–400, 1999. 6

83. R. Wegenkittl, A. Vilanova, B. Hegedüs, D. Wagner, M. Freund, and E. Gröller. Mastering Interactive Virtual Bronchioscopy on a Low-End PC. In *Proc. of IEEE Visualization*, pages 461–465, 2000. 3, 4, 7, 8

84. D. Welte and U. Klose. Segmentation and Selective Imaging of Arteries and Veins from Contrast-Enhanced MRA Data. In *Proc. of European Congress of Radiology*, 1999. 16

85. R. Westermann and T. Ertl. Efficiently Using Graphics Hardware in Volume Rendering Applications. In *Proc. of ACM SIGGRAPH*, pages 169–177, 1998. 2

86. L. Westover. Footprint Evaluation for Volume Rendering. In *Proc. of ACM SIGGRAPH*, pages 367–376, 1990. 2

87. R. Yagel and A. Kaufman. Template-based Volume Viewing. In *Proc. of Eurographics*, pages 153–167, 1992. 4

88. R. Yagel, D. Stredney, G. Wiet, P. Schmalbrock, L. Rosenberg, D. Sessanna, and Y. Kurzion. Building a Virtual Environment for Endoscopic Sinus Surgery Simulation. *Computers & Graphics*, 20(6):813–823, 1996. 3

89. S. You, L. Hong, M. Wan, K. Junyapreasert, A. Kaufman, S. Muraki, Y. Zhou, M. Wax, and Z. Liang. Interactive Volume Rendering for Virtual Colonoscopy. In *Proc. of IEEE Visualization*, pages 343–346, 1997. 4, 6

90. K. Zuiderveld, A. Koning, and M. Viergrever. Acceleration of Ray Casting Using 3D Distance Transform. In *Proc. of Visualization in Biomedical Computing*, pages 342–335, 1992. 6